Testing the impacts of wildfire on hydrological and sediment response using the OpenLISEM model. Part 1: Calibration and evaluation for a burned Mediterranean forest catchment

Jinfeng Wu[1,2,4,*] , João Pedro Nunes[2,3], Jantiene E. M. Baartman[2], C.A. Faúndez Urbina[5]

[1]State Key Laboratory of Hydroscience and Engineering, Department of Hydraulic Engineering, Tsinghua University, Beijing 100084, China

[2] Soil Physics and Land Management Group, Wageningen University and Research, P.O. Box 47, 6700 AA Wageningen, the Netherlands

[3] CE3C–Centro de Ecologia, Evolução e Alterações Climáticas, Faculdade de Ciências, Universidade de Lisboa, 1749-016 Lisboa, Portugal

[4] College of Land Science and Technology, China Agricultural University, Beijing 100193, China

[5] Instituto de Ciencias Agroalimentarias Animales y Ambientales, Universidad de O'Higgins, Ruta 90 Kilómetro 3, San Fernando, Chile

* Corresponding author:

E-mail: jinfengwu2020@163.com

Highlights

The spatially-distributed OpenLISEM model was applied to a burnt catchment.

Remote sensing and topographic analysis were substitute for field-based estimates.

The model was automatically calibrated for individual storms.

The model was validated using the jack-knife cross-validation procedure.

The model also predicted the spatial patterns of soil erosion.

This is the peer-reviewed version of the following article:

Wu J., Nunes J.P., Baartman J.E.M., Faúndez Urbina C.A. 2021. Testing the impacts of wildfire on hydrological and sediment response using the OpenLISEM model. Part 1: Calibration and evaluation for a burned Mediterranean forest catchment. Catena 207: 105658 (DOI: 10.1016/j.catena.2021.105658).

which has been published in final form at http://dx.doi.org/10.1016/j.catena.2021.105658.

Abstract

Models are typically applied to estimate the potential adverse effects of fire on land degradation and water resources and the potential benefits of post-wildfire rehabilitation treatments. However, few modeling studies have been conducted for meso-scale catchments, and only a fraction of these studies include transport and deposition of eroded material within the catchment or represent spatial erosion patterns. This study presents an application and evaluation of the OpenLISEM physically-based and spatially-distributed hydrological and soil erosion model for a burned Mediterranean meso-scale catchment (18.5 km^2) in a data-scarce environment, using a robust parameterization and calibration procedure: (1) integrating satellite imagery and the topographic wetness index to support model parameterization; (2) event-based automated calibration using the Model-Independent Parameter Estimation and Uncertainty Analysis and parameters ensemble for before and after the fire; (3) a jack-knife cross-validation for model evaluation. The study shows that this procedure used in OpenLISEM provides reasonable results for pre- and post-wildfire catchment discharge and sediment transport (r^2 and NSE > 0.5; absolute PBIAS < 25% for discharge and 55% for sediment transport). This may serve the needs of model applications in data-scarce burned areas. The results also provide recommended model parameters for burned areas with high severity such as random roughness (rr) = 2.41cm, and slope manning's n (n) = 0.038; or post-wildfire to pre-wildfire ratios of model parameters such as saturated hydraulic conductivity (K_s) = 0.98×, channel manning's n (chn) = 0.44×, grain size (d50) = 0.61×. The simulation results indicate that wildfire did not lead to significantly enhanced hydrological responses and soil erosion at the catchment outlet, partly explained by the spatial patterns of soil erosion. For both pre- and post-wildfire conditions, higher soil erosion was simulated in areas located far from the catchment outlet. The wildfire led to enhanced hillslope erosion, mostly in the upper part of the catchment, providing ample opportunities for transported sediment to deposit before reaching the outlet.

Keywords: Hydrological events, Soil erosion, Model calibration, Jack-knife cross-validation, Catchment scale

1 Introduction

Wildfires are common disturbances in Mediterranean forests (Pausas *et al.*, 2009; Shakesby, 2011; Verkaik *et al.*, 2013). Fires consume above-ground vegetation and soil cover, and after the wildfire, highly erodible fine ash is deposited on the soil surface (Zavala *et al.*, 2014). Fires also induce changes in soil structure, soil water repellency, and aggregate stability through soil heating and organic matter combustion (Mataix-Solera *et al.*, 2011; Zavala *et al.*, 2014). These changes in burned areas lead to enhanced hydro-sedimentary responses, resulting in land degradation and downstream water pollution, particularly in headwater forests (Moody *et al.*, 2013; Nunes *et al.*, 2018a; Smith *et al.*, 2011; Verkaik *et al.*, 2013). Moreover, the hydro-sedimentary impacts of wildfires may be more severe in a climate change context that implies an increase in the frequency and intensity of wildfires in Mediterranean forests in the future (Calheiros *et al.*, 2021; Morán‐Ordóñez *et al.*, 2020; Pausas *et al.*, 2009; Shakesby, 2011).

Accordingly, accurate predictions of post-wildfire hydro-sedimentary response to rainfall are needed to estimate the potential adverse effects of wildfire on land degradation and water resources, as well as the potential benefits of post-wildfire rehabilitation treatments (Moody *et al.*, 2013; Nunes *et al.*, 2018b; Shakesby, 2011). To date, most hydrological and erosion models developed for agricultural regions were tested and modified to simulate and predict the impacts of wildfire and post-wildfire rehabilitation treatments on hydrological response and soil erosion. These models used in fire-related runoff and erosion investigations are mainly classified into (1) hillslope-scale models, including USLE/RUSLE, MMF, PESERA, and ERMIT/WEPP in its hillslope version (Benavides-Solorio & MacDonald, 2005; Esteves *et al.*, 2012; Fernández & Vega, 2016; Fernández *et al.*, 2010; Hosseini *et al.*, 2018; Lanorte *et al.*, 2019; Larsen & MacDonald, 2007; Robichaud *et al.*, 2007; Soto & Díaz-Fierros, 1998; Vieira *et al.*, 2014; Vieira *et al.*, 2018; Zema *et al.*, 2020); (2) catchment-scale models based on representative elements, including ERMIT/WEPP in its catchment version, and SWAT (Basso *et al.*, 2019; Carvalho-Santos *et al.*, 2019; Nunes *et al.*, 2018b; Salis *et al.*, 2019); (3) catchment-scale models based on raster topography, such as LANDSOIL (Pastor *et al.*, 2019) and LISEM (Van Eck *et al.*, 2016).

Most models are applied to predict erosion at the microplot or plot scale, even when applied to large areas. For example, the empirical RUSLE and physically-based PESERA models have been applied in a large-scale burned Mediterranean catchment to predict post-wildfire soil losses (Karamesouti *et al.*, 2016); however, they only provide information for gross erosion in

each pixel and do not consider sediment transport and deposition within the catchment (i.e., net erosion), despite being applied at the watershed scale.

The SWAT and WEPP/ERMIT models have both been modified to estimate sediment delivery in burned Mediterranean basins (Basso *et al.*, 2019; Carvalho-Santos *et al.*, 2019; Salis *et al.*, 2019). However, these studies do not accurately represent the spatial patterns of catchments since they consider "representative elements" and not the morphology and topography directly as do raster grids, so connectivity is not explicitly represented (Nunes *et al.*, 2018c). To our knowledge, the only published application of a raster model to predict erosion in burned areas is that of LANDSOIL (Pastor *et al.*, 2019), albeit to a small 1 km^2 headwater catchment. However, the empirical nature of LANDSOIL makes it difficult to ensure appropriate simulations for other, larger catchments without calibration data. In addition, most models adapted for burned areas are not validated or assessed for uncertainties due to the scarcity of measured data (Lopes *et al.*, 2020). To our knowledge, in the Mediterranean area, only two studies reported both pre-fire and post-fire hydrological and soil erosion processes at the catchment scale (Nunes *et al.*, 2020; Wu *et al.*, 2020); datasets from other burnt areas in north America and Australia are not likely to be representative of Mediterranean conditions (Nunes *et al.*, 2018a). However, these datasets are needed to test models in both unburnt and burnt conditions, and ensure that model parameters can be correctly modified to represent the disturbance caused by fires.

The physically-based OpenLISEM model was developed to simulate catchment-scale hydrological and erosion processes, and has been applied to simulate post-wildfire discharge in a small burned area by Van Eck *et al.* (2016). These authors reported reasonable accuracy in predictions of total and peak discharge at the micro catchment scale (0.1 km^2). In the present work, we build on this previous study to test OpenLISEM to explicitly simulate sediment connectivity patterns before and after a fire at a larger spatial scale. We applied the model to a meso-scale burned catchment (Odeáxere: 18.53 km^2) located in southwestern Iberia, for which hydro-sedimentary data in burnt and unburnt conditions exists (Wu *et al.*, 2020). The objectives of this study were 1) to parameterize OpenLISEM using satellite imagery and the topographic wetness index; 2) to design an approach to calibrate OpenLISEM for pre- and post-fire events, including automated calibration, sensitivity analysis, and jack-knife cross-validation.

To this end, this study, firstly, integrated satellite-vegetation data with OpenLISEM parameterization; secondly, sensitivity analysis and autocalibration were performed using the Model-Independent Parameter Estimation and Uncertainty Analysis (PEST); thirdly, we

developed and applied a jack-knife cross-validation procedure to validate the ability of the OpenLISEM model to predict the hydrological and erosive response at the catchment scale.

2 Study area

The study was conducted in the Odeáxere catchment of southern Portugal (37.27º N, -8.67º W). The region has a hot-summer Mediterranean climate (Csa in the Köppen-Geiger classification) (Kottek *et al.*, 2006) with average annual temperatures varying between 20°C and 25°C. The average annual precipitation is 624 mm concentrated in a wet season from October to March.

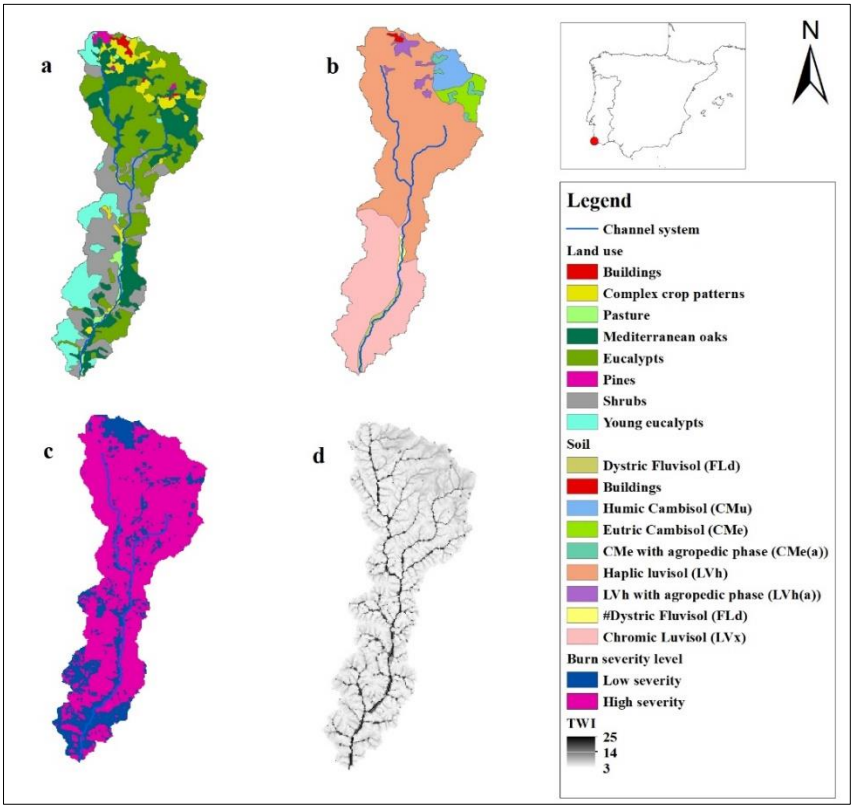

Figure 1 Study area with maps of: a) land use; b) soil type; c) burn severity level; and d) the topographic wetness index (TWI).

The catchment area is 18.53 km^2, which is between 10 and 1000 km^2; therefore, we used the term ‘meso-scale catchment’ in this study (Keesstra et al., 2009; Melland et al., 2018; Singh & Stenger, 2018; Uhlenbrook et al., 2004). Slope steepness varies from 0 to 36%, with an average of 16%. The study area is mainly covered by forests (69%) and shrubs (21%) (COS, 2007). The

forest area is mainly composed of Eucalypt plantations (34%), Mediterranean evergreen oak forests (22%), young Eucalypts (12%), and Pines (1%) (Fig. 1a). Note that this study used COS2007 as it was the closest available high-resolution landcover for the study period since the other was COS1995. The main soil types are Haplic Luvisols (LVh) (55%) and Chromic Luvisols (LVx) (32%), which account for about 87% of the catchment (Fig. 1b). The fire regime in the region belongs to the southwestern Iberia pyro-region (Calheiros *et al.*, 2020). The hydrological and erosion response is typical for the western Mediterranean region (Peña-Angulo *et al.*, 2019). Almost the entire surface area of the catchment burned in early August 2003 (Wu *et al.*, 2020), which provides an interesting case study to analyze the hydrological consequences of wildfire at the meso-catchment scale. About 78% of the area was burned with high severity; the remaining 22% was burned with low severity or not at all (Fig 1c, with moderate-low and moderate-high severities classified as low and high severities, respectively) (Wu *et al.*, 2020).

3 Methods

3.1 OpenLISEM model

The OpenLISEM model is a physically-based hydrological model (De Roo & Jetten, 1999; De Roo *et al.*, 1996a; De Roo *et al.*, 1996b) which is usually applied to catchment sizes ranging from 1 ha to 100 km^2 (Baartman *et al.*, 2012; De Roo & Jetten, 1999; Grum *et al.*, 2017; Van Eck *et al.*, 2016). The model simulates hydrological processes, including interception, ponding, infiltration, overland flow, and channel flow. Soil erosion processes include detachment by rainfall, throughfall, overland flow, transport capacity, and deposition. The model also optionally takes into account the influence of tractor wheeling, paved roads, hard surfaces, and water or sediment barriers (De Roo *et al.*, 1996a; De Roo *et al.*, 1996b). However, the model does not include slower processes, such as evapotranspiration, interflow, and groundwater flow, because it is designed to simulate the effects of land-use changes or conservation measures during heavy rainstorms. The infiltration rate is calculated by a two-layer Green-Ampt method, based on the Darcy equation for one-dimensional flow; in this study, infiltration in channel beds was set to zero. The model offers a choice of equations for soil erosion: the equations originating from the EUROSEM model were used for simulating sediment detachment and delivery in this study.

3.2 OpenLISEM parameterization

3.2.1 Initial parameterization

OpenLISEM needs various input maps categorized as catchment maps, land use maps, surface maps, soil characteristics, infiltration-related maps, and channel maps. All input maps had a resolution of 25m and were based on land use classes (Table 1), soil types (Table 2), and the permanent channel system. The 25m DEM was derived from the 10m Digital Elevation Model of the Portuguese Geographic Institute - IGP, which was then used to derive the slope steepness map and the location of the outlet. With aerial photography from Google Earth, the permanent channel system in the catchment (Fig. 1a) and its dimensions (width: 3-4m and depth: 0.32-0.43m) were constructed using ArcGIS. Besides, channel cohesion was calculated based on slope root cohesion and soil cohesion, and the channels Manning's n was set to 0.035.

Table 1 An overview of the input parameters that were based on the land use classes

Land use	Litter (-)	Vegetation height (m)	Random roughness (cm)	Manning's n	Root cohesion (kPa)
Buildings	0.00	4.00	1.87	0.11	8.26
Complex crop patterns	0.00	4.00	1.87	0.11	8.26
Pasture	0.00	0.50	1.22	0.41	3.41
Mediterranean oaks	0.50	6.00	1.50	0.32	26.60
Eucalypts	0.35	10.00	1.19	0.30	10.00
Pines	0.35	10.00	1.02	0.40	5.90
Shrubs	0.50	2.00	1.12	0.27	8.26
New Eucalypts	0.50	2.00	1.95	0.13	2.05

Notes: Values were based on Cronshey (1986) (Manning's n)； and Ferreira (1996); Nunes *et al.* (2017); Nunes *et al.* (2016); Nunes *et al.* (2018b); Nunes *et al.* (2009); Nunes *et al.* (2008); Serpa *et al.* (2015); Valente *et al.* (1997) (other parameters related to land use)

3.2.2 Manual parameter adjustment for burned conditions

Input parameters were adjusted for post-wildfire conditions using a simplified classification of low and high severity (Fig. 1c). Here, input parameters were adjusted in the burned areas with high severity. Litter cover (-) and vegetation height (m) were set to zero. Random roughness was assumed to have increased to 2.11 cm, and Manning's n was set to 0.05, both according to Van Eck *et al.* (2016). Root cohesion was left unchanged, as it was assumed the roots would still be intact enough to provide some cohesion in the soil. Besides, the saturated hydraulic conductivity (K_s) was assumed to have decreased; pre-fire K_s values were accordingly adjusted

by being multiplied by 0.37 based on Ebel and Moody (2020), but note that these were further adapted during model calibration (see section 4.3).

Table 2 An overview of the input parameters based on soil types for soil layers 1 and 2, respectively

	Fraction covered by stones	Cohesion (kPa)	Aggregate Stability	D50 (mu)	D90 (mu)	Saturated Hydraulic Conductivity (mm/h) (layer 1/layer 2)	Wetting front suction (cm) (layer 1/layer 2)	Porosity (layer 1/layer 2)	depth (cm) (layer 1/layer 2)
FLd	0.00	12.90	26.09	26.63	221	16.89/22.94	23.00/19.81	0.45/0.44	45/85
Buildings	0.18	25.24	59.00	66.00	980	2.15/4.23	16.44/99.20	0.40/0.38	20/40
CMu	0.00	22.70	20.18	97.59	760	9.05/14.33	9.41/8.74	0.45/0.49	45/91
CMe	0.06	13.44	19.04	92.51	1245	13.34/4.18	10.80/12.90	0.44/0.48	40/60
CMe(a)	0.00	10.08	19.04	92.51	1245	13.34/4.18	10.80/12.90	0.44/0.48	40/60
LVh	0.18	25.24	59.25	65.53	980	2.15/4.23	16.44/99.20	0.40/0.38	20/40
LVh(a)	0.00	18.93	59.25	65.53	980	2.15/4.23	16.44/99.20	0.40/0.38	20/40
#FLd	0.13	12.67	28.66	18.37	724	14.08/6.93	19.89/25.98	0.46/0.49	35/40
LVx	0.46	21.68	45.80	3.27	450	2.60/2.15	29.29/77.03	0.49/0.51	15/35

Notes: Dystric Fluvisol (FLd); Humic Cambisol (CMu); Eutric Cambisol (CMe); CMe with agropedic phase (CMe(a)); Haplic Luvisol (LVh); LVh with agropedic phase (LVh(a)); Similar to FLd (#FLd); Chromic Luvisol (LVx). Among soil erosion factors, texture, stone fraction, aggregate stability, *K*sat, porosity, and depth were taken from soil sample data for southern Portugal (de Carvalho Cardoso, 1965); Wetting front suction was calculated from texture following Rawls *et al.* (1983); Cohesion was taken from Rachman *et al.* (2003); D50 and D90 were calculated from texture following Skaggs *et al.* (2001).

3.2.3 Pre-storm soil moisture content

Since expanding saturated areas controlled by topographical properties have been reported during the wet season in this region, the topographic wetness index (TWI) was considered adequate for estimating soil moisture deficit at the beginning of each event, following the approach proposed by Nunes *et al.* (2009) based on the TWI formulations by Beven (2011). The spatial distribution of TWI is shown in Fig. 1d, which shows that areas with high index values prone to saturation are more concentrated along the main channel.

3.2.4 Vegetation cover

Satellite-vegetation information can be considered a suitable substitute for ground-based measurements for OpenLISEM parameterization (Van Eck *et al.*, 2016) and was therefore used in this study. Following the approach of Van Eck *et al.* (2016), leaf area index (LAI) values and the fraction of soil cover by the canopy (PER) were estimated using the NDVI images close to the simulated rainfall event attained from https://earthexplorer.usgs.gov/.

3.3 OpenLISEM calibration and validation

3.3.1 Selection of hydrological events for calibration and validation

A total of 37 hydrological events (27 pre-wildfire events and 10 post-wildfire events) were recorded between October 2001 and September 2004, spanning two hydrological years before the wildfire and one hydrological year after the wildfire (Wu *et al.*, 2020). Since the model was developed to simulate hydrological and soil erosion processes during heavy rainstorms, long-duration, low-intensity rainfall events were excluded from the further analyses in this study. Small events are also more challenging to simulate than larger events (Nearing, 2006), and large high-intensity events generally cause most erosion. Therefore, we focused on the relatively larger storms for model calibration (7 pre-wildfire events and 5 post-wildfire events), which led to quicker and higher runoff generation with more suspended sediment after the fire as compared to before the fire (Wu *et al.*, 2020). Detailed characteristics of the selected storms can be found in the supplementary material Table S.1. Note, however, that after calibrating the model for these large storms, the model was also run for all smaller storms to evaluate the model's performance for these small storms, even though they are less important in terms of runoff and sediment contribution (supplementary material Fig S.4).

3.3.2 Model calibration and validation approach

The 'estimation module' in the Model-Independent Parameter Estimation and Uncertainty Analysis (PEST) package (Doherty, 2018) was used for parameter estimation. Using these parameters, each storm was calibrated automatically using PEST. PEST estimates the parameter values by minimizing an objective function (Φ) computed as the sum of squared weighted residuals between model outputs and field measurements. Parameter bounds are needed for adjustable parameter scaling. In this study these were chosen based on the range of parameter values for land use classes and soil input data (Table 3). The parameter estimation procedure is described in more detail in Appendix A.

3.3.3 Model calibration

A sensitivity analysis was done using PEST to identify a subset of the most sensitive parameters for automated calibration (Takken *et al.*, 1999). The model was firstly calibrated for each event individually, based on outlet discharge (Q, l/s), peak discharge (Qpeak, l/s) and sediment load in the discharge (Qs, kg/s).

Table 3 Range for the adjustable parameters related to land use and all soil families (multiplication factor over the original parameter)

Land use					All soil families				
Obs	Adjustable parameters	Initial value	Lower bound	Upper bound	Obs	Adjustable parameters	Initial value	Lower bound	Upper bound
Q	Random roughness (rr, cm)	1.0	0.23	1.53	Q	Saturated hydraulic conductivity (*Ks*, mm/h)	1.0	0.23	37.43
Q	Leaf area index (LAI, m^2/m^2)	1.0	0.65	1.50	Q	Initial soil moisture content (thetai, -)	0.55 * θ_s	0.40 * θ_s	0.98 * θ_s
Q & Qs	Manning's n of slope (n, -)	1.0	0.50	1.85	Q	Wetting front suction (psi, cm)	1.0	0.32	10.98
Q & Qs	Manning's n of channel (chn, -)	1.0	0.50	1.85	Qs	Grain size (d50, mu)	1.0	0.08	29.69
					Qs	Cohesion (coh, kPa)	1.0	0.16	1.86
					Qs	Cohesion of channel (chc, kPa)	1.0	0.16	1.86
					Qs	Aggregate stability (ags, -)	1.0	0.06	2.26

Notes: values related to land use were taken from literature (Cronshey, 1986; Ferreira, 1996; Nunes *et al.*, 2017; Nunes *et al.*, 2016; Nunes *et al.*, 2018b; Nunes *et al.*, 2009; Nunes *et al.*, 2008; Serpa *et al.*, 2015; Valente *et al.*, 1997); values related to soil were derived from literature (de Carvalho Cardoso, 1965; Nunes *et al.*, 2008).

Secondly, the parameters from the autocalibrated individual storms were combined into two ensemble parameter sets, one for pre-fire conditions and another for post-fire conditions (Fig. 2). The weight of the parameters from each individual storm calibration in the ensemble was calculated using the prior and posterior likelihoods of each storm (Beven & Binley, 1992; McIntyre *et al.*, 2005), where the prior likelihood is related with storm magnitude and the posterior likelihood is related with the width of the 95% confidence interval of the autocalibrated parameter. The calculation of prior and posterior likelihoods is further described in Appendix A.

Thus, parameter *i* of each ensemble parameter set ($\overline{Sp_i}$) was computed as follows:

$$\overline{Sp_i} = \sum_{j=1}^{n} Sp_{ij} \times \omega_{ij} \qquad \text{Eq. 1}$$

Where n is the number of storms for the ensemble parameter set, $\overline{Sp_i}$ is the ensemble value of autocalibrated parameter *i*, Sp_{ij} is the autocalibrated multiplication factor for adjustable parameter *i* of storm *j* obtained by applying automated calibration using PEST, and ω_{ij} is the product of the prior and posterior likelihood for autocalibrated parameter *i* of storm *j*.

3.3.4 Jack-knife cross-validation procedure and model performance

In the jack-knife procedure, one storm at a time was treated as a validation event, while the autocalibrated parameters of the remaining storms were used to build a new ensemble parameter set to be tested (Fig. 2). The evaluation focused on the main output variables of hydro-

sedimentary response: total response, peak response, and time to peak response, both for discharge and sediment transport.

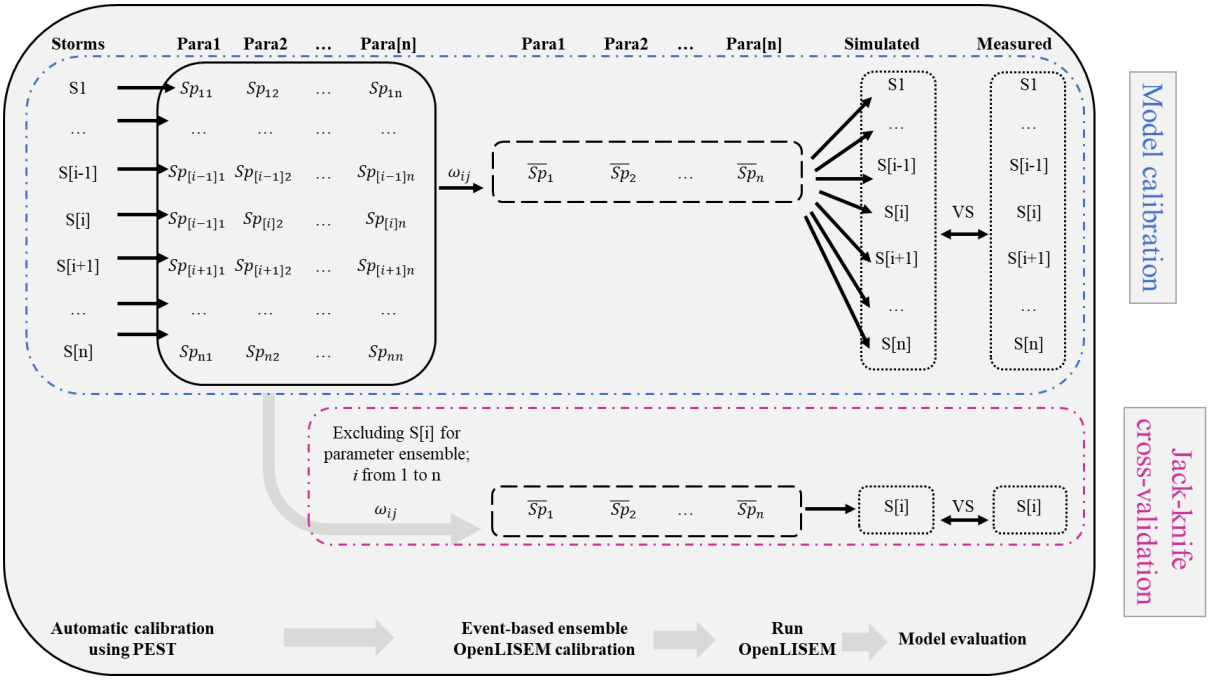

Figure 2 Procedures of model calibration and jack-knife cross-validation

Model performance was evaluated using the coefficient of determination (r^2) and the Nash-Sutcliffe model efficiency (NSE) (Moriasi *et al.*, 2015; Nunes *et al.*, 2009). R^2 values above 0.5 for discharge and 0.4 for sediment transport indicates reasonable model performance. NSE values higher than 0.5 indicates satisfactory model performance. In addition, percent bias (PBIAS) was calculated to indicate the magnitude of model errors compared to measurements. Positive PBIAS values indicate model overestimation and negative values indicate model underestimation. For daily simulations, absolute PBIAS values below 25% for discharge, and below 55% for sediment transport are considered reasonable (Moriasi *et al.*, 2015).

4 Results

4.1 Sensitivity analysis

Observations of discharge (Q), peak discharge (Qpeak), and sediment transport (Qs) for all storms were evaluated in the sensitivity analysis (Fig. 3). It can be concluded that, for all

observations, saturated hydraulic conductivity (K_s) and the manning's n of slope and channel (n and chn) are the most sensitive parameters. Random roughness (rr), grain size (d50), the cohesion of slope and channel (coh and chc), and aggregate stability (ags) are also important parameters. OpenLISEM is less sensitive to changes in initial water content (θ_i), wetting front suction (psi), and leaf area index (LAI).

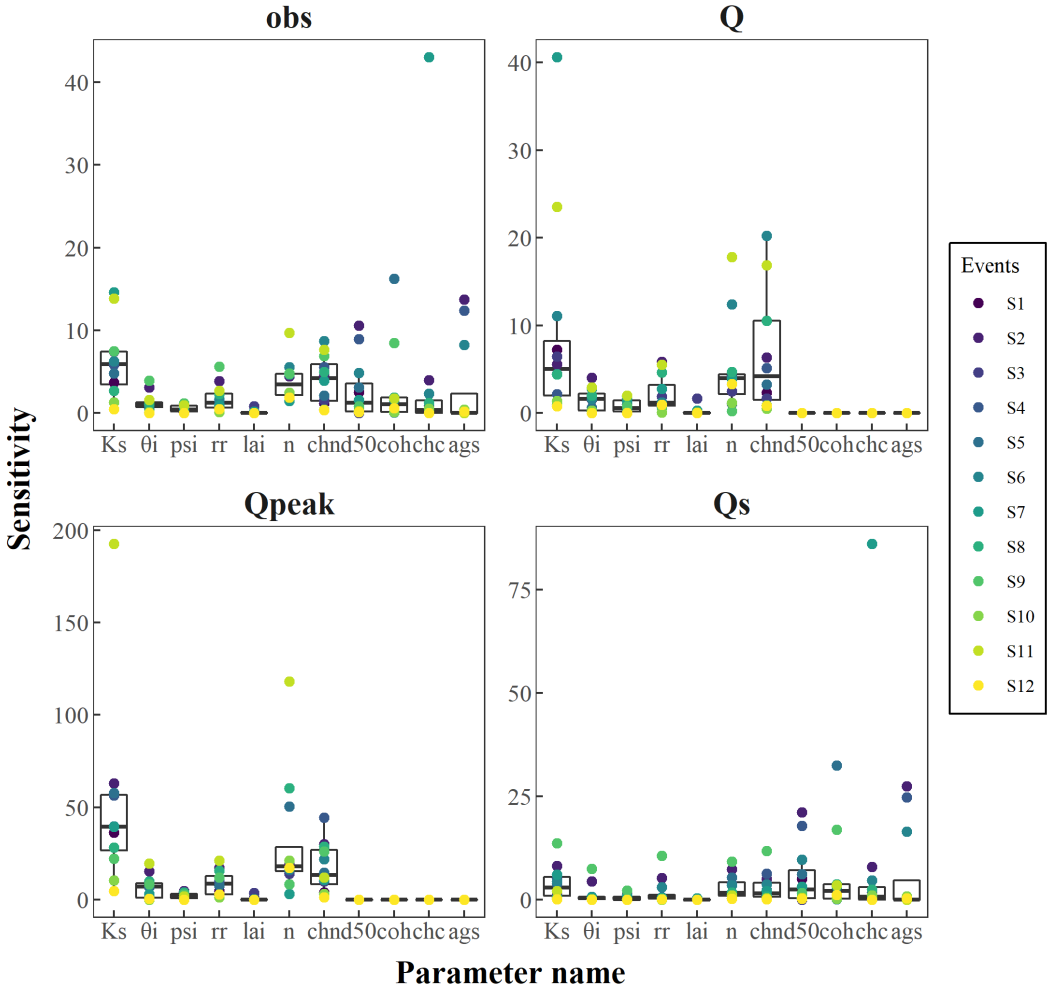

Figure 3 OpenLISEM parameters sensitivity analysis

The most sensitive parameters for Q and Qpeak are K_s, n, and chn. However, Qpeak appears to be more sensitive to changes in most parameters. Qs seems to be less sensitive to all parameters, although it is relatively sensitive to changes in K_s, d50, and coh. Note that the relatively higher sensitivity of Qs to K_s can be explained because Qs unilaterally depends on Q.

4.2 Calibration for individual storms

Based on the sensitivity analysis, the adjustable parameters, K_s, n, chn, and rr were used for Q calibration. The parameters d50, coh, chc, and agrs were used for Qs calibration. Since Qs unilaterally depends on Q, as mentioned above, the model was firstly calibrated for Q.

Fig. 4 shows the optimized multiplication factors and the 95% confidence limits of adjustable parameters for each individual event after automated calibration. Overall, autocalibrated parameters are consistent within the 95% confidence limits. For the calibrated K_s multiplication factor, most pre-wildfire storms belong to the group with lower multiplication and narrow margins, and most post-wildfire storms belong to a group with higher optimized multiplication factor and wide margins; but it should be noted that post-fire K_s were assumed to be lower than pre-fire K_s at the start. The same occurs for coh. As for n and chn multiplication factors, most pre-wildfire storms belong to a group with a higher optimized multiplication factor, and most post-wildfire storms belong to a group with a lower optimized multiplication factor, with relatively wide margins in both cases. As for other adjustable parameters (rr, d50, chc, and ags), there is no apparent difference between pre- and post-wildfire storms.

Table 4 shows OpenLISEM performance after automated calibration for individual events. As can be seen, the model shows satisfactory performance for almost all selected storms except S7 in accordance to the model performance criteria ($r^2 > 0.5$ for Q and 0.4 for Qs; NSE > 0.5). This indicates that OpenLISEM does not simulate the hydro-sedimentary response of S7 correctly within the allowable bounds of the adjustable parameters. Besides, the discharge of pre-wildfire storms S3 and S7 and post-wildfire storms S9 (absolute PBIAS < 25%) was underestimated.

The measured versus simulated results of the total, peak, and time to peak hydro-sedimentary response of all storms shows good results after automated calibration (r^2 and NSE > 0.5), in accordance to the model performance criteria (in the supplementary material Fig. S.1). The absolute PBIAS for simulated hydro-sedimentary response is considered reasonable. Again, it is evident that S7 can be considered an outlier according to the simulated result of time to peak discharge, possibly due to a mismatch in the timing of available rainfall data with streamflow data, e.g., the rain gauge was not representative of catchment conditions for this particular storm. Thus, S7 was excluded from event-based ensemble OpenLISEM calibration and jack-knife cross-validation.

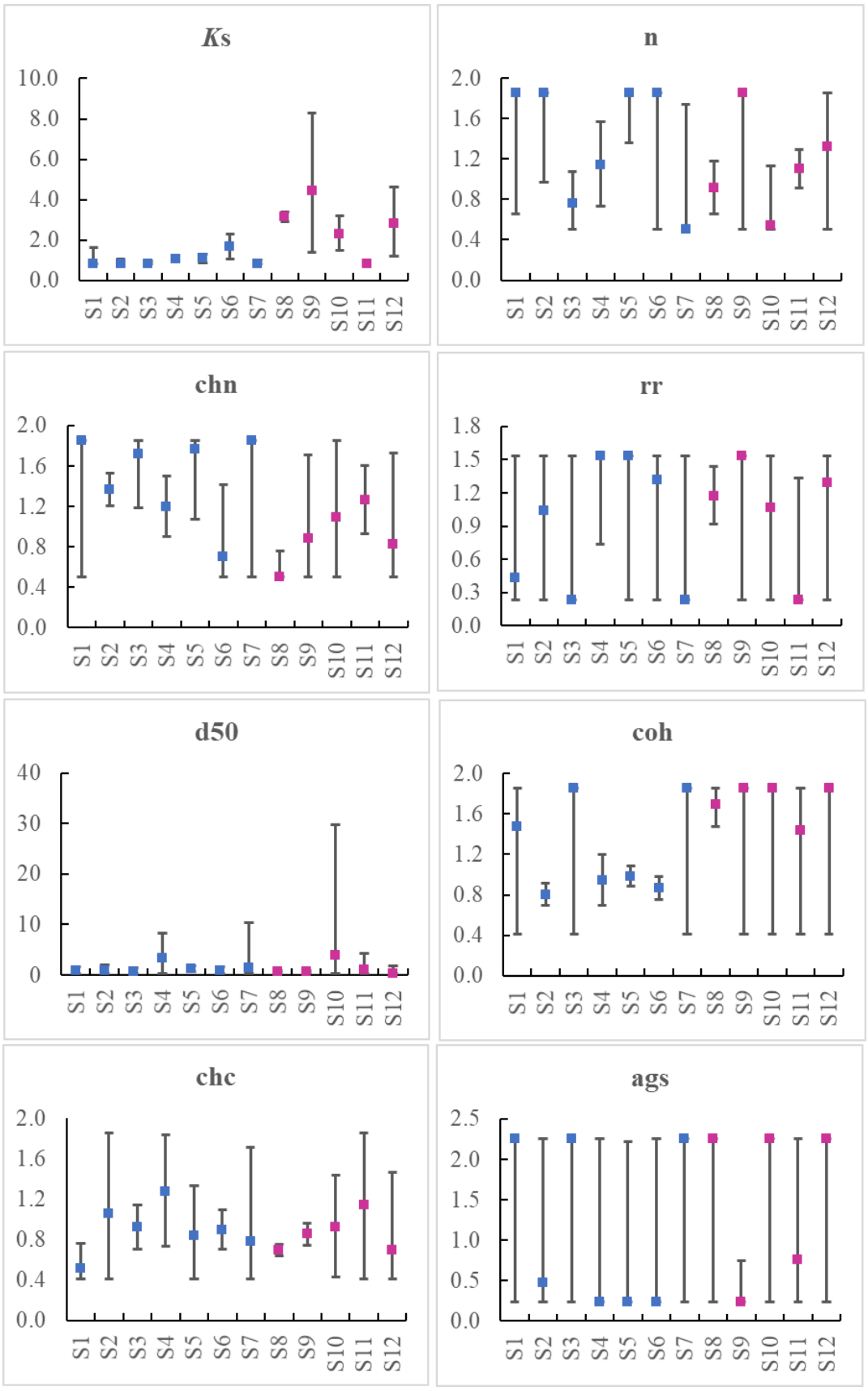

Figure 4 Adjustable parameters multiplication factor of each individual storm after automated model calibration (square-dots represent optimized values; bars represent the 95% confident limits)

Table 4 OpenLISEM performance for automated calibration optimization results of individual events

		S1	S2	S3	S4	S5	S6	S7	S8	S9	S10	S11	S12
Q	r^2	0.66	0.95	0.86	0.97	0.95	0.96	0.57	0.99	0.61	0.87	1.00	0.78
	NSE	0.65	0.94	0.81	0.97	0.94	0.95	0.22	0.99	0.51	0.87	0.97	0.73
	PBIAS	-5.90	-7.70	-29.30	-7.00	15.30	-7.50	-45.50	2.20	-39.70	2.70	-16.10	-8.60
Qs	r^2	0.77	0.77	0.82	0.96	0.99	0.93	0.07	0.99	0.95	0.74	0.65	0.63
	NSE	0.76	0.77	0.76	0.96	0.99	0.93	-0.11	0.99	0.95	0.68	0.58	0.57
	PBIAS	14.50	-13.80	-13.10	-3.30	-3.30	-5.30	-27.70	4.20	-3.80	-19.00	-35.50	-24.70

4.3 Calibration with pre- and post-fire ensemble parameter sets

Table 5 shows calibrated values for the adjustable parameters both before and after the fire. Firstly, the calibrated multiplication factors and spatial mean values for rr, chc, and ags were almost the same for pre- and post-wildfire conditions. These are the least sensitive parameters in OpenLISEM. Secondly, for the most sensitive adjustable parameters, it can be noted that: (1) after the fire, the multiplication factor for calibrated K_s is 2.61, which contrasts with the assumed decrease of K_s as a result of fire (equaling 0.37*pre-wildfire K_s); (2) after the fire, the spatial mean values of K_s and chc are 4.63 and 15.44, increasing by 37% and 85%, respectively, compared to before the fire; (3) after the fire, the spatial mean values of n, chn and d50 are 0.07, 0.02, and 27.96, decreasing by 84% and 60%, and 39%, respectively.

Table 5 Multiplication factors for calibrated parameters. The spatial mean value of the parameters is given between brackets.

	Pre-wildfire	Post-wildfire
*K*s	0.99 (3.37)	2.61 (4.63)
n	1.67 (0.45)	0.76 (0.07)
chn	1.33 (0.05)	0.59 (0.02)
rr	1.53 (2.13)	1.14 (2.27)
d50	0.97 (46.16)	0.59 (27.96)
coh	0.92 (8.34)	1.70 (15.44)
chc	0.78 (10.29)	0.77 (10.23)
ags	0.23 (11.50)	0.23 (11.50)

As can been seen in Fig. 5, the event-based ensemble OpenLISEM calibration shows good performance for pre-and post-wildfire hydro-sedimentary response at the catchment outlet. Besides, absolute PBIAS for simulated results of hydro-sedimentary response is considered reasonable.

There are no noticeable differences for OpenLISEM performance in discharge simulations between before and after the fire. The results are consistent for both before and after the fire, with the best fit for time to peak discharge and increasingly worse performance for total discharge and, subsequently, for peak discharge. However, while model performance for pre-wildfire discharge and sediment transport was similar, the performance for post-wildfire sediment was worse than that for post-wildfire discharge. Moreover, performance for post-wildfire sediment transport was worse than for pre-wildfire sediment. According to Fig. 5, this relatively lower model performance after wildfire is mostly related to underestimating total sediment transport and peak sediment transport in the biggest storm S10.

As for the prediction of individual events using the ensemble calibration parameter set for before and after the fire, OpenLISEM does not show satisfactory performance for every storm. R^2 values were reasonable in most cases ($r^2 > 0.5$ for Q and 0.4 for Qs), but NSE values only indicated satisfactory model performance (NSE > 0.5) for hydrograph prediction in six storms (4 before and 2 after fire) and for sedigraph prediction in three storms (2 before and 1 after fire).

A similar decrease in model accuracy was found in the jack-knife cross-validation phase, with better performance for pre-wildfire conditions than for post-wildfire, and also better for discharge than for sediment transport, especially after the fire. These results are detailed in the supplementary material (Tables S.4 and S.5, and Fig. S.2 and S.3).

Despite these limitations in simulating individual hydrographs and sedigraphs, model performance was still considered satisfactory in distinguishing the total hydro-sedimentary response of different storms before and after the fire (Fig. 5).

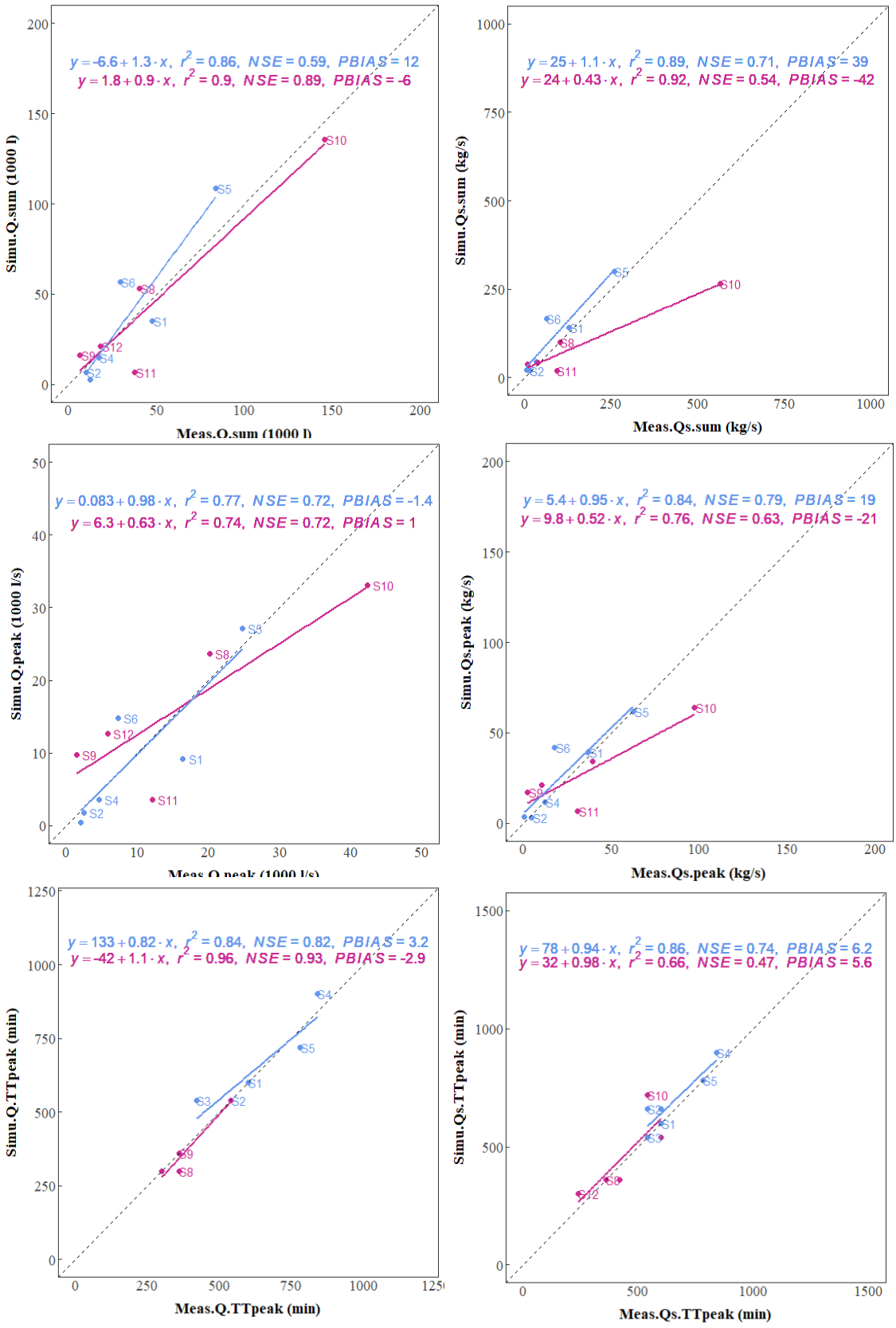

Figure 5 Model performance in catchment hydro-sedimentary response simulations after OpenLISEM calibration for before (blue) and after (purple) the fire

4.4 Soil erosion spatial patterns

To explore the impacts of wildfire on soil erosion and deposition patterns, the simulated soil erosion and deposition patterns (divided by rainfall amount) (Malvar et al., 2013; Malvar et al., 2016; Prats et al., 2019; Vieira et al., 2015) for before and after the fire are shown in Fig. 6. For both pre- and post-wildfire conditions, higher soil erosion was simulated in the stream and in the area with complex crop patterns located in the upper part of the catchment. Deposition mainly occurs in the riparian areas close to the main stream. By comparison, after the fire, relatively higher soil erosion was simulated in both complex crop patterns and on the hillslopes with high burn severity; however, it is evident that higher hillslope erosion also mainly occurs in the upper part of the catchment, which in normal (unburnt) conditions is less connected with the catchment outlet as compared with the middle and lower part.

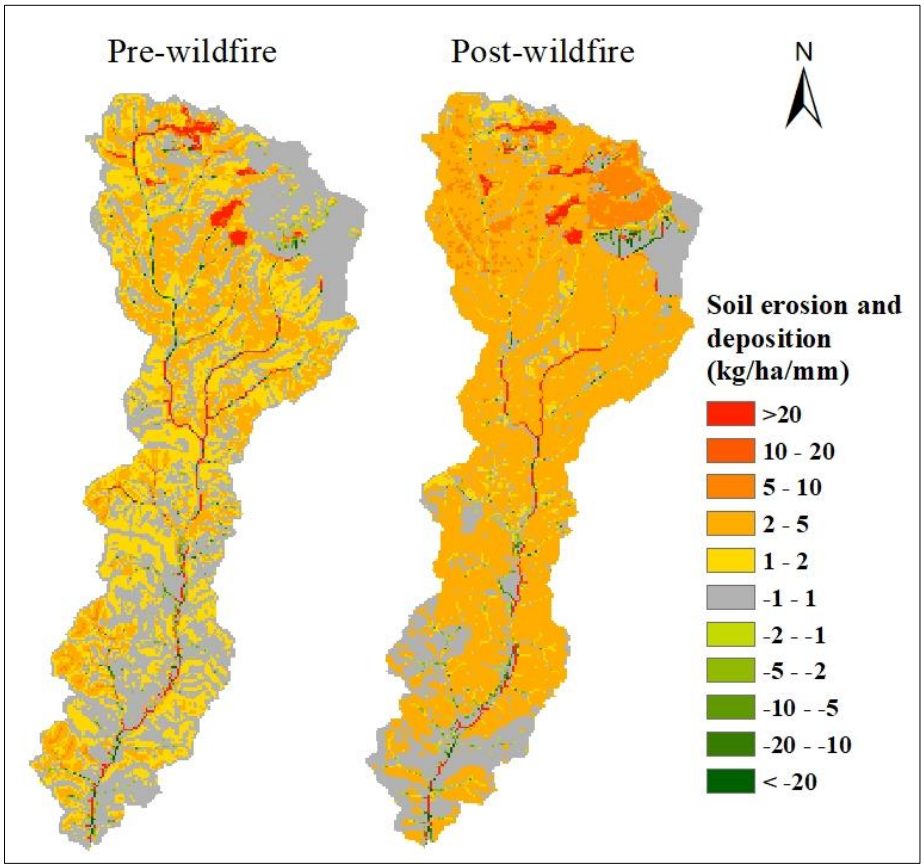

Figure 6 Simulated soil erosion and deposition pattern (divided by rainfall amount) before and after the fire

5 Discussion

5.1 Modelling and parameterization

Our findings show that, for hydrological processes, the OpenLISEM model is most sensitive to changes in K_s, n, and chn. For erosion processes, it is most sensitive to changes in K_s, d50, and coh. However, the sensitivity of the parameters varies from storm to storm and between observation groups (Q, Qpeak, Qs). This was also found in other studies (De Roo *et al.*, 1996a; Jetten *et al.*, 1998; Sheikh *et al.*, 2010; Van Eck *et al.*, 2016). For example, peak discharge is more sensitive to changes in these calibrated parameters, which indicates that more focus should be given to peak discharge during calibration.

In contrast, OpenLISEM is not sensitive to changes in LAI when simulating the impacts of vegetation on hydrological and erosion processes. This is consistent with Van Eck *et al.* (2016), who found OpenLISEM showed little sensitivity to the interception simulation due to the model itself and the low interception rates of plantation forests. Using satellite imagery to estimate vegetation cover values for OpenLISEM can therefore be a reliable alternative to costly field-based estimates, especially for larger catchments and when timeseries are required to assess vegetation recovery.

De Roo and Jetten (1999) reported that OpenLISEM was sensitive to changes in θ_i, especially to small changes in θ_i when reaching saturation. This was not found in our study, probably because our catchment is much larger than the small 45 ha catchment analysed by De Roo and Jetten (1999). The result indicates that OpenLISEM is not sensitive to the methods used to introduce θ_i. Therefore, TWI and a TOPMODEL-based approach can be considered a suitable substitute for fieldwork-based measurements to spatialize pre-storm θ_i, especially in a data-scarce environment. Besides, Nunes *et al.* (2009) found that TWI and a TOPMODEL-based approach to spatialize pre-storm θ_i can decrease uncertainty in a similar model; therefore, in this context, the method was applied to support OpenLISEM parameterization.

5.2 Model performance and limitations

In this study, the OpenLISEM model was applied for the first time to a burned Mediterranean meso-scale catchment (18.5 km^2) in order to improve the understanding of fire-induced hydrological changes and spatial soil erosion patterns. In this study, model parameterization was based on land use and soil data from maps and existing databases, and on satellite imagery

and TWI estimations, but not including local field sampling of e.g. soil properties. Although we think that field estimations would certainly have helped increase insight in local conditions, the size of the catchment requires using maps and upscaling local measurements also with local measurements. In addition, fieldwork is generally hard to plan in fire-related studies, as it is impossible to predict where and when a fire will occur (Shakesby, 2011). To overcome the data availability limitation, a robust parameterization and calibration procedure was presented: (1) integrating satellite imagery and TWI to support model parameterization, (2) event-based automated calibration with PEST and parameters ensemble for before and after wildfire; (3) a jack-knife cross-validation for model evaluation. It should be highlighted, however, that automated parameter estimation using PEST requires the undertaking of many model runs, which represents a considerable numerical burden (Doherty, 2018). Therefore, in order to ease numerical burden, 25m resolution maps were used instead of 10m resolution since the model runs more than 20x faster using 25m as compared to 10m resolution. To assess the differences between the resolutions, we ran the model at 10m resolution using the parameter set that was calibrated for 25m and we found there were almost no differences in spatial patterns of soil loss (see details in the supplementary material (Fig. S.5)). This is consistent with Hessel (2005), who also suggested the model performance at 10m and 20m resolution is similar, unlike at 50m and larger.

OpenLISEM successfully simulated total discharge, peak discharge, and total sediment transport before and after wildfire at the catchment outlet. The exception was sediment transport of the largest storm after the fire, partly explained with measurement uncertainty, as peak turbidity values were outside the calibration sensor range (Wu *et al.*, 2020). Nevertheless, the model showed an acceptable performance for the main output variables of pre-and post-wildfire hydro-sedimentary responses.

With the model calibration and validation results, we concluded that OpenLISEM was able to simulate catchment total and peak discharge and total sediment transport before and after wildfire satisfactorily. However, this conclusion has some limitations. Firstly, OpenLISEM is a physically-based model, simulating multiple hydrological and erosion processes based on a large set of input data. This allows for a good representation of the catchment, and can help understand complex hydrological and erosion processes, and especially how they can be impacted by wildfire. However, increasing the number of processes will increase the data requirements of the model, which will increase the uncertainty of simulated values (Batista *et al.*, 2019; Jetten *et al.*, 1999; Takken *et al.*, 1999). In this study, input data uncertainty can be

attributed to: (1) rainfall, including time step of rainfall intensity and the spatial distribution of rainfall. As K_s is the most sensitive parameter, different rainfall intensities will lead to different overland flow generation rates, with large consequences for simulation results. For example, when the model was automatically calibrated for individual storms using PEST, S7 was considered to be an outlier, which can partially be explained by the uncertainty of spatial information of rainfall intensity for this particular storm. (2) Input parameters related to land use and soil types. While input data were taken from representative profiles for southern Portugal, calibration was done for the existing spatial pattern of land use and soil types, not for each patch of land or soil, resulting in some amount of uncertainty.

Secondly, no model is entirely comprehensive, and in this case, OpenLISEM does not incorporate interflow and groundwater flow processes; therefore, the long-duration storms have been excluded from the modelling study. This is similar to other event-driven hydrological models, and it has been shown that slower processes are not critical at an event level (De Roo & Jetten, 1999). More importantly, the simulation of saturated overland flow that occurs during wet conditions was limited since θ_i was an insensitive parameter, which may contribute a lot to runoff generation in this catchment (Wu *et al.*, 2020).

Thirdly, although OpenLISEM is a spatially distributed erosion model, it was calibrated using discharge and sediment transport data collected at the catchment outlet. Compared with Van Eck *et al.* (2016), who applied the model to a smaller Portuguese catchment, OpenLISEM performed considerably better for overall model performance, with higher r^2 and NSE above the thresholds for satisfactory or good model performance. This could be explained by the larger size catchment, probably due to an averaging effect (De Roo & Jetten, 1999; Takken *et al.*, 1999). Again, it indicates outlet calibration and evaluation can mask significant spatial variation within the catchment, but unfortunately, in this study, we lack the data to confirm or deny this (Batista *et al.*, 2019).

Finally, OpenLISEM performed considerably better for discharge than for sediment delivery, particularly after the fire. This is consistent with Jetten *et al.* (1999), who also suggested that discharge is better predicted than sediment transport. In this study, it can be partly explained by the autocalibrated procedure using PEST in which we performed discharge calibration first, followed by sediment transport calibration. Besides, it should be noted that the method of ensemble parameter set calculation was partly based on storm magnitude, because large high-

intensity events not only play an important role in model calibration, but are also responsible for a large part of hydrological response and soil erosion.

5.3 Impact of wildfire on hydrological and erosion processes

Wildfire did alter catchment hydrological and erosion processes, which can be reflected in changes to spatial mean values of calibrated parameters after wildfire compared to before wildfire, such as K_s, n, chn, d50, and coh. As expected, compared with pre-wildfire, after a wildfire, n and chn decreased by above 60%, which leads to the faster hydrological response after a wildfire as compared to before wildfire, as can be seen in Fig. 5.

However, unexpectedly, post-wildfire events had higher spatial mean values of K_s when compared with pre-wildfire events. Our initial estimate of post-wildfire K_s was 0.37 * pre-wildfire K_s following field study results (Ebel & Moody, 2020), but the autocalibration proposed a multiplication factor of this K_s of 2.61 (the pre-wildfire K_s itself was multiplied by 0.99). The end result is that post-wildfire K_s equals 0.98 * pre-wildfire K_s.

One immediate conclusion is that, in future applications of OpenLISEM, K_s should not be decreased as a result of a wildfire. This contrasts with the conclusions of Ebel and Moody (2020), which may be related to scale differences; while Ebel and Moody (2020) reached their conclusions based on point infiltration measurements, OpenLISEM assumes cell-wide homogenous values (25*25m^2) where the presence of high infiltration patches might counteract the fire effect (see (Nunes *et al.*, 2018c)). In this particular case, this can be related to the scale issues surrounding the effect of soil water repellency on post-wildfire hydrological and erosion processes (see Langhans *et al.* (2016)). Soil water repellency has been commonly observed after fires, including in Mediterranean forests, enhancing runoff generation and, consequently, soil erosion (Moody *et al.*, 2013; Shakesby, 2011). On the one hand, wildfire can induce and enhance soil water repellency and, on the other hand, induce macropore flow due to processes such as root burning. Therefore, Ferreira *et al.* (2005) and Martínez-Zavala and Jordán-López (2009) also suggested the patchy patterns of occurrence and persistence of soil water repellency can be modulated by other factors such as post-wildfire macropores when the scale becomes wider. This mechanism might explain the difference between the point measurements of Ebel and Moody (2020) and the parameterization of K_s in the 25*25 m^2 cells used in this study.

Another factor that might explain these differences is the uncertainty of the hydrological effects of the ash layer that remains on the soil surface after the wildfire. On the one hand, it has been shown that clogging and sealing topsoil pores by fine ash particles leads to reduced infiltration (Stoof *et al.*, 2016). On the other hand, Moody *et al.* (2009) reported higher values of near-K_s for soil with ash than in soil unaffected by the fire; Woods and Balfour (2008) pointed out the final runoff rate was lower, and the total infiltration was higher than in the plots without ash; Stoof *et al.* (2010) demonstrated direct incorporation of ash into soils did not alter soil texture but increased water retention.

Changes in d50 and coh after wildfire were both related to soil erosion processes. Decreasing d50 may lead to an increase in soil erosion, while increasing cohesion can limit soil loss. Decreased d50 after a fire may be because we are simulating ash and fine sediments from forest soils. Unexpectedly, as compared to before fire, there is a higher cohesion after a fire. One possible explanation would be this compensates for the appearance of stones after a few erosion events (Shakesby, 2011). Moreover, input parameters in the burned areas, including LAI, PER, litter cover, and vegetation height, were adjusted for post-wildfire conditions, which means there was increased fine sediment supply after the wildfire.

Nevertheless, these changes in the burned areas did not lead to significantly enhanced sediment yield as would be expected. While the fire led to higher soil erosion rates in the burned areas (Fig. 6), the highest soil erosion rates after the wildfire were still simulated in the area with complex crop patterns, as was the case in pre-wildfire conditions. All these high erosion areas are not well connected with the catchment outlet when compared to the middle and lower part of the catchment. Again, this indicates that other factors can moderate the impacts of wildfire on hydrological and erosion response at large scales, and is consistent with the observations of Wu *et al.* (2020) who attributes the limitation of post-wildfire soil erosion to transport-limited sediment yield, rather than to detachment limitations.

When compared with other modelling studies referred earlier, this work contrasts in two main aspects: the negligible impact of fire on the runoff generation ratio and on sediment yield. From our arguments above, it follows that these differences can be related with the relatively large gridcell size (25m) when compared with microplots and plots used in other model studies, and also the larger size of the Odeaxere catchment (18 km^2) compared with those of other studies (typically under 1 km^2). A larger cell size includes within-cell patchiness of soil water repellency partly negating its effects on runoff generation, and a larger catchment includes burnt

headwater catchments which are not well connected to the main channel. More modelling studies for larger catchments would help assess and verify these differences.

5.4 Implications

Our study shows the potential to apply an event-driven model to study hydrological and erosion processes in burnt catchments in data scarce environments using a robust calibration procedure. Our approach uses event-based automatic calibrating using PEST, to limit biases in the assumed parameter values for post-fire conditions; and a jack-knife procedure to allow cross-validation despite scarce data. It would be interesting to apply this procedure to other larger catchments and assess similarities and differences in the autocalibrated parameters, although the scarcity of comparative pre- and post-fire data for burnt areas will probably limit the availability of a dataset for this purpose.

Our study also reinforces the usefulness of satellite imagery to derive vegetation cover information for spatially-distributed modelling, as described in previous studies; and provides a calibrated parameter set (Table 5) for a burnt Mediterranean catchment, which might be replicated in other studies where post-fire parameter information is lacking, which is often the case. In particular, the relative parameter changes between pre- and post-fire conditions might be applicable elsewhere, such as the strong decrease in flow resistance and particle size, the strong increase in soil cohesion and surface storage, and (in contrast to other studies) the limited changes to soil hydraulic conductivity.

6 Conclusions

The OpenLISEM model was tested for discharge and sediment transport predictions before and after wildfire using storms that occurred during two hydrological years before the wildfire and one hydrological year after the wildfire. Overall, the model showed an acceptable performance for the main output variables of pre-and post-wildfire hydro-sedimentary response through model performance evaluation and jack-knife cross-validation. Comparatively speaking, OpenLISEM had a better performance for pre-wildfire hydro-sedimentary response predictions than for post-wildfire predictions, in particular for sediment yield. After the wildfire, a relatively lower model performance was mostly related to underestimating total sediment yield and peak sediment transport in the biggest storm.

The wildfire did alter catchment hydrological and erosion processes, reflected in changes to spatial mean values of calibrated parameters after wildfire, such as LAI, n, and d50. Contrary to observations at the patch scale, calibrated values for K_s did not change with the wildfire, possibly due to the relatively large size of model cells and the study catchment, which mitigates small-scale effects.

Wildfire did not significantly enhance sediment yield at the catchment outlet. In both pre- and post-wildfire conditions, higher soil erosion was simulated in the area with complex crop patterns located far from the catchment outlet; moreover, enhanced hillslope erosion after wildfire also mainly occurs in the upper part of the catchment. These areas are not well-connected with the outlet, and the model results indicate a transport limitation on sediment yield.

Overall, this study presents an application and evaluation of the OpenLISEM model for a burned area in a data-scarce environment, using a robust parameterization and calibration procedure: (1) integrating satellite imagery and TWI to support model parameterization, (2) event-based automated calibration using PEST and parameter ensembles for before and after wildfire; (3) a jack-knife cross-validation for OpenLISEM model evaluation, which suggests a potentially broader application. It also proposes fire impacts on hydrological parameters in similar models applied at a similar spatial scale. We suggest that typical values, such as LAI = 0, rr = 2.41cm, n = 0.038, could be used to scale burned areas with high severity. Besides, ratios of post- to pre-wildfire model parameters such as saturated K_s = 0.98×, chn = 0.44×, d50 = 0.61× could be used for model parameterization. Subsequently, an accompanying paper elaborates on the implications of storm frequency and magnitude for post-wildfire erosion using the calibrated OpenLISEM model.

Acknowledgments

The China Scholarship Council funded this work through the grant attributed to J Wu (CSC: 201806350161). Additional funding was obtained from the Portuguese Fundação para a Ciência e a Tecnologia, through support attributed to JP Nunes: individual grant IF/00586/2015, project FRISCO (PCIF/MPG/0044/2018), and funding attributed to the CE3C research center (UIDB/00329/2020). C.A. Faúndez Urbina thanks the Comisión Nacional de Investigación Científica y Tecnológica, CONICYT PFCHA/Doctorado Becas Chile/2015 – 72160322. The authors would like to acknowledge Luis Dias and Inês Morais for helping with data collection and preparation.

Appendix A

Pre-storm moisture content computation

The average soil moisture deficit at the beginning of each event was estimated based on initial baseflow at the beginning of the runoff event, using the following equation (Eq. 1):

$$Q_i = A * e^{-Y} * e^{-\frac{D}{m}} \qquad \text{Eq. 1}$$

with Q_i baseflow before the storm (m^3 h^{-1}), A catchment area (m^2), Y average topographic wetness index value for the catchment, D average soil moisture deficit for the catchment (m), m the decay of hydraulic transmissivity with soil profile depth.

Then, D_x soil moisture deficit at point x (m) was calculated as (Eq. 2),

$$D_x = D + m * (Y - Y_x) \qquad \text{Eq. 2}$$

with Y_x topographic wetness index value at point x.

LAI and PER computation

$$LAI = -K^{-1} * LN\left(\left(NDVI - NDVI_{\max\_LAI}\right) * \left(NDVI_{\min\_LAI} - NDVI_{\max\_LAI}\right)^{-1}\right) \qquad \text{Eq. 3}$$

where *K* is the light extinction coefficient specific to each vegetation type, ranging between 0.8 and 1.4 (Baret & Guyot, 1991).

The fraction of soil cover by the canopy (PER) was also calculated from the light extinction coefficient (Eq. 4) using the LAI maps (Deguchi *et al.*, 2006).

$$PER = 1 - EXP(-K * LAI) \qquad \text{Eq. 4}$$

Parameter estimation and sensitivity analysis

PEST achieves automated calibration of individual events through changing model adjustable parameters to minimize the objective function (Φ) by a Gauss-Marquardt-Levenberg method.

$$\Phi = \sum_i^m (w_i r_i)^2 \qquad \text{Eq. 5}$$

where Φ represents the objective function, m is the number of observations, w_i is the weight associated with the *i*th observation, and r_i is the *i*th residual (difference between model-simulated output and measurement). In this study, observations at the catchment outlet (obs)

were divided into three groups: discharge (Q, l/s), peak discharge (Qpeak, l/s), and sediment transport (Qs, kg/s), which can facilitate calculation of the weights (w_i) because the magnitude of discharge (Q) and sediment transport (Qs) was somewhat different.

During optimization processes, PEST calculates the Jacobian matrix and then estimates the relative comprehensive sensitivity of each parameter. The value reflects the input parameters' sensitivity to the objective function, in which a higher value represents a higher response to the objective function. The formula is as follows (Eq. 6),

$$s_i = \left(J^t \bullet Q \bullet J\right)_{ii}^{1/2} / m \qquad \text{Eq. 6}$$

Where, s_i is the comprehensive sensitivity of the ith parameter, and m is the weighted average of observations. Note that K_s was used for Q calibration, not for Qs calibration, although it is also the most sensitive parameters for Qs. There are three reasons: (1) Sediment transport was well related to water discharge for this catchment according to event-based analysis (Pearson's correlation coefficient, $p < 0.05$); (2) after automatic calibration, we got the optimized value and the 95% confident limits of adjustable parameters; as for model calibration, we took two factors into consideration: the 95% confident limits of adjustable parameters and storm magnitude; (3) PEST achieves automated calibration of individual events through changing model adjustable parameters to minimize the objective function (Φ) by a Gauss-Marquardt-Levenberg method, which requires no more than 4 adjustable parameters for each parameters estimation, otherwise there is no solution or considerable uncertainty about the results.

Prior and posterior likelihoods (ω_{ij}) computation

The prior likelihood of storms, E_j, represents the applicability of the autocalibrated parameter set of storm *j* prior to considering high-intensity storms commonly held responsible for the main part of the hydrological response and soil erosion. It integrates parameters into the ensemble set according to storm magnitude. In this study, E_j was quantified in terms of the normalized event index (EVI = (total rainfall * IP30max) / rainfall duration) measure of the candidate storms (i.e., all E_i sum to unity).

The relative posterior likelihood, B_{ij}, quantifies the applicability of autocalibrated parameter *i* of storm *j* based on the 95% confidence limits of automated calibration. This was done to give

a higher weight for parameters with narrow limits, as parameters with wide confidence limits can be more widely adjusted without decreasing model performance. It was computed as:

$$B_{ij} = \frac{1-\frac{CI_{ij}}{CI_{max}}}{\sum_{j=1}^{n}(1-\frac{CI_{ij}}{CI_{max}})} \qquad \text{Eq. 7}$$

Where CI_{ij} is the distance between lower and upper limits within 95% confidence of autocalibrated parameter i of storm j, CI_{max} is the maximum value of CI_{ij}.

The likelihood of parameter i, ω_{ij}, was then computed by:

$$\omega_{ij} = \frac{E_j B_{ij}}{\sum_{j=1}^{n} E_j P_{ij}} \qquad \text{Eq. 8}$$

All the ω_{ij} values sum to unity.

References

Baartman, J. E., Jetten, V. G., Ritsema, C. J., de Vente, J., 2012. Exploring effects of rainfall intensity and duration on soil erosion at the catchment scale using openLISEM: Prado catchment, SE Spain. Hydrological Processes 26(7), 1034-1049.

Baret, F., Guyot, G., 1991. Potentials and limits of vegetation indices for LAI and APAR assessment. Remote sensing of environment 35(2-3), 161-173.

Basso, M., Vieira, D. C. S., Ramos, T. B., Mateus, M., 2019. Assessing the adequacy of SWAT model to simulate postfire effects on the watershed hydrological regime and water quality. Land Degradation & Development 31(5), 619-631. 10.1002/ldr.3476.

Batista, P. V., Davies, J., Silva, M. L., Quinton, J. N., 2019. On the evaluation of soil erosion models: Are we doing enough? Earth-Science Reviews 197, 102898.

Benavides-Solorio, J. d. D., MacDonald, L. H., 2005. Measurement and prediction of post-fire erosion at the hillslope scale, Colorado Front Range. International Journal of Wildland Fire 14(4), 457-474. https://doi.org/10.1071/WF05042.

Beven, K., Binley, A., 1992. The future of distributed models: model calibration and uncertainty prediction. Hydrological Processes 6(3), 279-298.

Beven, K. J., 2011. Rainfall-runoff modelling: the primer: John Wiley & Sons.

Calheiros, T., Nunes, J. P., Pereira, M. G., 2020. Recent evolution of spatial and temporal patterns of burnt areas and fire weather risk in the Iberian Peninsula. Agricultural and Forest Meteorology 287. https://doi.org/10.1016/j.agrformet.2020.107923.

Calheiros, T., Pereira, M. G., Nunes, J. P., 2021. Assessing impacts of future climate change on extreme fire weather and pyro-regions in Iberian Peninsula. Sci Total Environ 754, 142233. https://doi.org/10.1016/j.scitotenv.2020.142233.

Carvalho-Santos, C., Marcos, B., Nunes, J., Regos, A., Palazzi, E., Terzago, S., Monteiro, A., Honrado, J., 2019. Hydrological Impacts of Large Fires and Future Climate: Modeling Approach Supported by Satellite Data. Remote Sensing 11(23). https://doi.org/10.3390/rs11232832.

De Roo, A., Jetten, V., 1999. Calibrating and validating the LISEM model for two data sets from the Netherlands and South Africa. Catena 37(3-4), 477-493.

De Roo, A., Offermans, R., Cremers, N., 1996a. LISEM: A single - event, physically based hydrological and soil erosion model for drainage basins. II: Sensitivity analysis, validation and application. Hydrological Processes 10(8), 1119-1126.

De Roo, A., Wesseling, C., Ritsema, C., 1996b. LISEM: a single - event physically based hydrological and soil erosion model for drainage basins. I: theory, input and output. Hydrological Processes 10(8), 1107-1117.

Deguchi, A., Hattori, S., Park, H.-T., 2006. The influence of seasonal changes in canopy structure on interception loss: Application of the revised Gash model. Journal of Hydrology 318(1-4), 80-102. https://doi.org/10.1016/j.jhydrol.2005.06.005.

Doherty, J. (Ed.), 2018. Model-independent parameter estimation user manual.

Ebel, B. A., Moody, J. A., 2020. Parameter estimation for multiple post - wildfire hydrologic models. Hydrological Processes. 10.1002/hyp.13865.

Esteves, T. C. J., Kirkby, M. J., Shakesby, R. A., Ferreira, A. J. D., Soares, J. A. A., Irvine, B. J., Ferreira, C. S. S., Coelho, C. O. A., Bento, C. P. M., Carreiras, M. A., 2012. Mitigating land degradation caused by wildfire: Application of the PESERA model to fire-affected sites in central Portugal. Geoderma 191, 40-50. 10.1016/j.geoderma.2012.01.001.

Fernández, C., Vega, J. A., 2016. Evaluation of RUSLE and PESERA models for predicting soil erosion losses in the first year after wildfire in NW Spain. Geoderma 273, 64-72. https://doi.org/10.1016/j.geoderma.2016.03.016.

Fernández, C., Vega, J. A., Vieira, D. C. S., 2010. Assessing soil erosion after fire and rehabilitation treatments in NW Spain: Performance of rusle and revised Morgan-Morgan-Finney models. Land Degradation & Development 21(1), 58-67. https://doi.org/10.1002/ldr.965.

Ferreira, A. J. D., Coelho, C. O. A., Boulet, A. K., Leighton-Boyce, G., Keizer, J. J., Ritsema, C. J., 2005. Influence of burning intensity on water repellency and hydrological processes at forest and shrub sites in Portugal. Soil Research 43(3), 327-336. https://doi.org/10.1071/SR04084.

Grum, B., Woldearegay, K., Hessel, R., Baartman, J. E. M., Abdulkadir, M., Yazew, E., Kessler, A., Ritsema, C. J., Geissen, V., 2017. Assessing the effect of water harvesting techniques on event-based hydrological responses and sediment yield at a catchment scale in northern Ethiopia using the Limburg Soil Erosion Model (LISEM). Catena 159, 20-34. 10.1016/j.catena.2017.07.018.

Hessel, R., 2005. Effects of grid cell size and time step length on simulation results of the Limburg soil erosion model (LISEM). Hydrological Processes: An International Journal 19(15), 3037-3049.

Hosseini, M., Nunes, J. P., Pelayo, O. G., Keizer, J. J., Ritsema, C., Geissen, V., 2018. Developing generalized parameters for post-fire erosion risk assessment using the revised Morgan-Morgan-Finney model: A test for north-central Portuguese pine stands. Catena 165, 358-368. 10.1016/j.catena.2018.02.019.

Jetten, V., De Roo, A., Favis-Mortlock, D., 1999. Evaluation of field-scale and catchment-scale soil erosion models. Catena 37(3-4), 521-541.

Jetten, V., de Roo, A., Guérif, J. (1998). Sensitivity of the model LISEM to variables related to agriculture. In *Modelling soil erosion by water* (pp. 339-349): Springer.

Karamesouti, M., Petropoulos, G. P., Papanikolaou, I. D., Kairis, O., Kosmas, K., 2016. Erosion rate predictions from PESERA and RUSLE at a Mediterranean site before and after a wildfire: Comparison & implications. Geoderma 261, 44-58. 10.1016/j.geoderma.2015.06.025.

Keesstra, S., Bruijnzeel, L., Van Huissteden, J., 2009. Meso - scale catchment sediment budgets: combining field surveys and modeling in the Dragonja catchment, southwest Slovenia. Earth Surface Processes and Landforms 34(11), 1547-1561.

Kottek, M., Grieser, J., Beck, C., Rudolf, B., Rubel, F., 2006. World Map of the Köppen-Geiger climate classification updated. Meteorologische Zeitschrift 15(3), 259-263. https://doi.org/10.1127/0941-2948/2006/0130.

Langhans, C., Smith, H. G., Chong, D. M. O., Nyman, P., Lane, P. N. J., Sheridan, G. J., 2016. A model for assessing water quality risk in catchments prone to wildfire. Journal of Hydrology 534, 407-426. https://doi.org/10.1016/j.jhydrol.2015.12.048.

Lanorte, A., Cillis, G., Calamita, G., Nolè, G., Pilogallo, A., Tucci, B., De Santis, F., 2019. Integrated approach of RUSLE, GIS and ESA Sentinel-2 satellite data for post-fire soil erosion assessment in Basilicata region (Southern Italy). Geomatics, Natural Hazards and Risk 10(1), 1563-1595. 10.1080/19475705.2019.1578271.

Larsen, I. J., MacDonald, L. H., 2007. Predicting postfire sediment yields at the hillslope scale: Testing RUSLE and Disturbed WEPP. Water Resources Research 43(11). https://doi.org/10.1029/2006wr005560.

Lopes, A., Girona - García, A., Corticeiro, S., Martins, R., Keizer, J., Vieira, D., 2020. What is wrong with post - fire soil erosion modelling? A meta - analysis on current approaches, research gaps, and future directions. Earth Surface Processes and Landforms.

Malvar, M. C., Martins, M. A., Nunes, J. P., Robichaud, P. R., Keizer, J. J., 2013. Assessing the role of pre-fire ground preparation operations and soil water repellency in post-fire runoff and inter-rill erosion by repeated rainfall simulation experiments in Portuguese eucalypt plantations. Catena 108, 69-83.

Malvar, M. C., Prats, S. A., Keizer, J. J., 2016. Runoff and inter - rill erosion affected by wildfire and pre - fire ploughing in eucalypt plantations of north - central Portugal. Land Degradation & Development 27(5), 1366-1378.

Martínez-Zavala, L., Jordán-López, A., 2009. Influence of different plant species on water repellency in Mediterranean heathland soils. Catena 76(3), 215-223. https://doi.org/10.1016/j.catena.2008.12.002.

Mataix-Solera, J., Cerdà, A., Arcenegui, V., Jordán, A., Zavala, L. M., 2011. Fire effects on soil aggregation: A review. Earth-Science Reviews 109(1-2), 44-60. https://doi.org/10.1016/j.earscirev.2011.08.002.

McIntyre, N., Lee, H., Wheater, H., Young, A., Wagener, T., 2005. Ensemble predictions of runoff in ungauged catchments. Water Resources Research 41(12). 10.1029/2005wr004289.

Melland, A., Fenton, O., Jordan, P., 2018. Effects of agricultural land management changes on surface water quality: A review of meso-scale catchment research. Environmental science & policy 84, 19-25.

Moody, J. A., Kinner, D. A., Úbeda, X., 2009. Linking hydraulic properties of fire-affected soils to infiltration and water repellency. Journal of Hydrology 379(3-4), 291-303. https://doi.org/10.1016/j.jhydrol.2009.10.015.

Moody, J. A., Shakesby, R. A., Robichaud, P. R., Cannon, S. H., Martin, D. A., 2013. Current research issues related to post-wildfire runoff and erosion processes. Earth-Science Reviews 122, 10-37. https://doi.org/10.1016/j.earscirev.2013.03.004.

Morán - Ordóñez, A., Duane, A., Gil - Tena, A., De Cáceres, M., Aquilué, N., Guerra, C. A., Geijzendorffer, I. R., Fortin, M. J., Brotons, L., 2020. Future impact of climate extremes in the Mediterranean: Soil erosion projections when fire and extreme rainfall meet. Land Degradation & Development. 10.1002/ldr.3694.

Moriasi, D. N., Gitau, M. W., Pai, N., Daggupati, P., 2015. Hydrologic and water quality models: Performance measures and evaluation criteria. Transactions of the ASABE 58(6), 1763-1785.
Nearing, M., 2006. 13 Can Soil Erosion be Predicted? Soil erosion and sediment redistribution in river catchments: measurement, modelling and management, 145.
Nunes, J. P., Bernard - Jannin, L., Rodríguez - Blanco, M. L., Boulet, A. K., Santos, J. M., Keizer, J. J., 2020. Impacts of wildfire and post - fire land management on hydrological and sediment processes in a humid Mediterranean headwater catchment. Hydrological Processes. https://doi.org/10.1002/hyp.13926.
Nunes, J. P., Doerr, S. H., Sheridan, G., Neris, J., Santín, C., Emelko, M. B., Silins, U., Robichaud, P. R., Elliot, W. J., Keizer, J., 2018a. Assessing water contamination risk from vegetation fires: Challenges, opportunities and a framework for progress. Hydrological Processes 32(5), 687-694. https://doi.org/10.1002/hyp.11434.
Nunes, J. P., Naranjo Quintanilla, P., Santos, J. M., Serpa, D., Carvalho-Santos, C., Rocha, J., Keizer, J. J., Keesstra, S. D., 2018b. Afforestation, Subsequent Forest Fires and Provision of Hydrological Services: A Model-Based Analysis for a Mediterranean Mountainous Catchment. Land Degradation & Development 29(3), 776-788. https://doi.org/10.1002/ldr.2776.
Nunes, J. P., Seixas, J., Keizer, J. J., Ferreira, A. J. D., 2009. Sensitivity of runoff and soil erosion to climate change in two Mediterranean watersheds. Part I: model parameterization and evaluation. Hydrological Processes 23(8), 1202-1211. 10.1002/hyp.7247.
Nunes, J. P., Wainwright, J., Bielders, C. L., Darboux, F., Fiener, P., Finger, D., Turnbull, L., 2018c. Better models are more effectively connected models. Earth Surface Processes and Landforms 43(6), 1355-1360.
Pastor, A. V., Nunes, J. P., Ciampalini, R., Koopmans, M., Baartman, J., Huard, F., Calheiros, T., Le-Bissonnais, Y., Keizer, J. J., Raclot, D., 2019. Projecting Future Impacts of Global Change Including Fires on Soil Erosion to Anticipate Better Land Management in the Forests of NW Portugal. Water 11(12). https://doi.org/10.3390/w11122617.
Pausas, J. G., Llovet, J., Rodrigo, A., Vallejo, R., 2009. Are wildfires a disaster in the Mediterranean basin?–A review. International Journal of Wildland Fire 17(6), 713-723. https://doi.org/10.1071/WF07151.
Peña-Angulo, D., Nadal-Romero, E., González-Hidalgo, J. C., Albaladejo, J., Andreu, V., Bagarello, V., Barhi, H., Batalla, R. J., Bernal, S., Bienes, R., Campo, J., Campo-Bescós, M. A., Canatario-Duarte, A., Cantón, Y., Casali, J., Castillo, V., Cerdà, A., Cheggour, A., Cid, P., Cortesi, N., Desir, G., Díaz-Pereira, E., Espigares, T., Estrany, J., Fernández-Raga, M., Ferreira, C. S. S., Ferro, V., Gallart, F., Giménez, R., Gimeno, E., Gómez, J. A., Gómez-Gutiérrez, A., Gómez-Macpherson, H., González-Pelayo, O., Hueso-González, P., Kairis, O., Karatzas, G. P., Klotz, S., Kosmas, C., Lana-Renault, N., Lasanta, T., Latron, J., Lázaro, R., Le Bissonnais, Y., Le Bouteiller, C., Licciardello, F., López-Tarazón, J. A., Lucía, A., Marín, C., Marqués, M. J., Martínez-Fernández, J., Martínez-Mena, M., Martínez-Murillo, J. F., Mateos, L., Mathys, N., Merino-Martín, L., Moreno-de las Heras, M., Moustakas, N., Nicolau, J. M., Novara, A., Pampalone, V., Raclot, D., Rodríguez-Blanco, M. L., Rodrigo-Comino, J., Romero-Díaz, A., Roose, E., Rubio, J. L., Ruiz-Sinoga, J. D., Schnabel, S., Senciales-González, J. M., Simonneaux, V., Solé-Benet, A., Taguas, E. V., Taboada-Castro, M. M., Taboada-Castro, M. T., Todisco, F., Úbeda, X., Varouchakis, E. A., Vericat, D., Wittenberg, L., Zabaleta, A., Zorn, M., 2019. Spatial variability of the relationships of runoff and sediment yield with weather types throughout the Mediterranean basin. Journal of Hydrology 571, 390-405. 10.1016/j.jhydrol.2019.01.059.
Prats, S. A., González - Pelayo, Ó., Silva, F. C., Bokhorst, K. J., Baartman, J. E., Keizer, J. J., 2019. Post - fire soil erosion mitigation at the scale of swales using forest logging residues at a reduced application rate. Earth Surface Processes and Landforms 44(14), 2837-2848.
Robichaud, P. R., Elliot, W. J., Pierson, F. B., Hall, D. E., Moffet, C. A., 2007. Predicting postfire erosion and mitigation effectiveness with a web-based probabilistic erosion model. Catena 71(2), 229-241. 10.1016/j.catena.2007.03.003.
Salis, M., Del Giudice, L., Robichaud, P. R., Ager, A. A., Canu, A., Duce, P., Pellizzaro, G., Ventura, A., Alcasena-Urdiroz, F., Spano, D., Arca, B., 2019. Coupling wildfire spread and erosion models to quantify post-fire erosion before and after fuel treatments. International Journal of Wildland Fire 28(9). https://doi.org/10.1071/wf19034.
Shakesby, R. A., 2011. Post-wildfire soil erosion in the Mediterranean: Review and future research directions. Earth-Science Reviews 105(3-4), 71-100. https://doi.org/10.1016/j.earscirev.2011.01.001.
Sheikh, V., van Loon, E., Hessel, R., Jetten, V., 2010. Sensitivity of LISEM predicted catchment discharge to initial soil moisture content of soil profile. Journal of Hydrology 393(3-4), 174-185. https://doi.org/10.1016/j.jhydrol.2010.08.016.
Singh, S. K., Stenger, R., 2018. Indirect methods to elucidate water flows and contaminant transfer pathways through meso-scale catchments–a review. Environmental Processes 5(4), 683-706.
Smith, H. G., Sheridan, G. J., Lane, P. N. J., Nyman, P., Haydon, S., 2011. Wildfire effects on water quality in forest catchments: A review with implications for water supply. Journal of Hydrology 396(1-2), 170-192. https://doi.org/10.1016/j.jhydrol.2010.10.043.
Soto, B., Díaz-Fierros, F., 1998. Runoff and soil erosion from areas of burnt scrub: comparison of experimental results with those predicted by the WEPP model. Catena 31(4), 257-270.
Stoof, C. R., Gevaert, A. I., Baver, C., Hassanpour, B., Morales, V. L., Zhang, W., Martin, D., Giri, S. K., Steenhuis, T. S., 2016. Can pore-clogging by ash explain post-fire runoff? International Journal of Wildland Fire 25(3), 294-305.
Stoof, C. R., Wesseling, J. G., Ritsema, C. J., 2010. Effects of fire and ash on soil water retention. Geoderma 159(3-4), 276-285. https://doi.org/10.1016/j.geoderma.2010.08.002.

Takken, I., Beuselinck, L., Nachtergaele, J., Govers, G., Poesen, J., Degraer, G., 1999. Spatial evaluation of a physically-based distributed erosion model (LISEM). Catena 37(3-4), 431-447.
Uhlenbrook, S., Roser, S., Tilch, N., 2004. Hydrological process representation at the meso-scale: the potential of a distributed, conceptual catchment model. Journal of Hydrology 291(3-4), 278-296.
Van Eck, C. M., Nunes, J. P., Vieira, D. C. S., Keesstra, S., Keizer, J. J., 2016. Physically - Based Modelling of the Post - Fire Runoff Response of a Forest Catchment in Central Portugal: Using Field versus Remote Sensing Based Estimates of Vegetation Recovery. Land Degradation & Development 27(5), 1535-1544. https://doi.org/10.1002/ldr.2507.
Verkaik, I., Rieradevall, M., Cooper, S. D., Melack, J. M., Dudley, T. L., Prat, N., 2013. Fire as a disturbance in mediterranean climate streams. Hydrobiologia 719(1), 353-382. https://doi.org/10.1007/s10750-013-1463-3.
Vieira, D., Fernández, C., Vega, J., Keizer, J., 2015. Does soil burn severity affect the post-fire runoff and interrill erosion response? A review based on meta-analysis of field rainfall simulation data. Journal of Hydrology 523, 452-464.
Vieira, D. C. S., Prats, S. A., Nunes, J. P., Shakesby, R. A., Coelho, C. O. A., Keizer, J. J., 2014. Modelling runoff and erosion, and their mitigation, in burned Portuguese forest using the revised Morgan–Morgan–Finney model. Forest Ecology and Management 314, 150-165. https://doi.org/10.1016/j.foreco.2013.12.006.
Vieira, D. C. S., Serpa, D., Nunes, J. P. C., Prats, S. A., Neves, R., Keizer, J. J., 2018. Predicting the effectiveness of different mulching techniques in reducing post-fire runoff and erosion at plot scale with the RUSLE, MMF and PESERA models. Environ Res 165, 365-378. 10.1016/j.envres.2018.04.029.
Woods, S. W., Balfour, V. N., 2008. The effect of ash on runoff and erosion after a severe forest wildfire, Montana, USA. International Journal of Wildland Fire 17(5), 535-548. https://doi.org/10.1071/WF07040.
Wu, J., Baartman, J. E. M., Nunes, J. P., 2020. Comparing the impacts of wildfire and meteorological variability on hydrological and erosion responses in a Mediterranean catchment. Land Degradation & Development 32(2), 640-653. https://doi.org/10.1002/ldr.3732.
Zavala, L. M. M., de Celis Silvia, R., López, A. J., 2014. How wildfires affect soil properties. A brief review. Cuadernos de investigación geográfica/Geographical Research Letters,(40), 311-331.
Zema, D. A., Nunes, J. P., Lucas-Borja, M. E., 2020. Improvement of seasonal runoff and soil loss predictions by the MMF (Morgan-Morgan-Finney) model after wildfire and soil treatment in Mediterranean forest ecosystems. Catena 188. https://doi.org/10.1016/j.catena.2019.104415.

Supplementary material

Table S.1 Characteristics of the selected storms for the model calibration and validation before and after the fire

	Storms	NDVI	API	Qi	Pdura	P	IP	IP30max	EVI	Rdura	Q	RC	Qstm	Qpeak	Qs	SSL
	No.	-	-	$m^3 s^{-1}$	h	mm	$mm h^{-1}$	$mm h^{-1}$	-	h	$m^3 s^{-1}$	-	$m^3 s^{-1}$	$m^3 s^{-1}$	$kg s^{-1}$	ton
Pre-wildfire	S1	0.76	8.42	0.05	12	31.45	2.62	16.76	13.25	14	3.39	0.28	5.25	17.41	8.61	433.98
	S2	0.68	29.34	0.83	12	11.83	0.99	12.30	43.92	10	0.98	0.16	2.38	3.67	1.30	46.87
	S3	0.64	37.73	0.56	13	15.94	1.23	7.10	12.13	14	0.88	0.15	2.07	3.07	0.32	15.90
	S4	0.73	33.65	0.47	14	21.14	1.51	10.83	8.71	18	0.94	0.15	1.93	5.72	1.80	116.78
	S5	0.75	13.78	0.27	18	51.37	2.85	18.11	16.35	12	6.97	0.31	9.86	29.66	19.38	837.08
	S6	0.70	0.95	0.09	14	38.64	2.76	18.25	51.68	13	2.26	0.14	3.48	8.82	4.60	215.39
	S7	0.69	4.46	0.61	18	35.95	2.00	5.27	50.36	20	1.81	0.19	3.96	6.67	1.82	131.26
Post-wildfire	S8	0.33	8.92	0.00	9	30.20	3.36	17.37	10.53	6	6.73	0.25	8.68	22.83	15.85	342.33
	S9	0.44	5.55	0.05	11	19.90	1.81	10.89	58.28	12	0.54	0.06	0.98	1.56	0.71	30.51
	S10	0.44	24.35	0.22	22	72.64	3.30	20.46	19.70	15	9.70	0.38	16.10	46.05	33.03	1783.78
	S11	0.45	24.09	0.98	9	15.33	1.70	5.63	67.55	11	3.41	0.46	5.75	14.59	3.56	140.95
	S12	0.45	11.97	0.39	10	17.41	1.74	12.57	9.59	7	2.57	0.31	4.06	7.03	4.83	121.68

Notes: The antecedent precipitation index (API, -) and initial baseflow (Qi, $m^3 s^{-1}$) were also included to describe antecedent conditions prior to each runoff event; API was calculated using the equation proposed by Kohler *et al.* (1951) and based on the rainfall of the previous 10 days;

Rainfall variables including rainfall duration (Pdura, h); rainfall amount (P, mm); rainfall intensity (IP, $mm h^{-1}$); maximum rainfall intensity in 30 min (IP30max, $mm h^{-1}$); the normalized event index (EVI, -); IP30max was calculated from maximum hourly rainfall, using existing relationships between hourly and 30 mins rainfall (Brandão *et al.*, 2001); multiply total rainfall and IP30max together divided by rainfall duration equals EVI;

Hydro-sedimentary variables including runoff duration (Rdura, h); surface discharge (Q, $m^3 s^{-1}$); runoff coefficient (RC, -); streamflow discharge (Qstm, %); peak discharge (Qpeak, $m^3 s^{-1}$). The transport of sediment by discharge was characterized by sediment transport (Qs, $kg s^{-1}$) and sediment yields (SSL, ton).

Since PEST does sensitivity analysis and parameter estimation automatically, it is important to set the bounds of the allowable values (i.e., physically meaningful) for each parameter (Table 3 & 4). The procedure for estimating the bounds of each parameter was as follows: firstly, a minimum and maximum value of each parameter for all land use or soil types in the catchment were derived through literature review, and then average statistic variable of minimum and

maximum of each parameter for the catchment were computed, including average, minimum, 1st Quartile, median, 3rd Quartile, and maximum. Finally, a conservative range and a wide range were recommended for PEST automatic calibration and sensitivity analysis. The lower and upper bounds of the conservative range represent median of minimum and maximum, respectively. The lower and upper bounds of the wide range represent the 1st Quartile of the minimum and the 3rd Quartile of the maximum, respectively.

Table S.2 Range for the adjustable parameters related to land use (multiplication factor over the original parameter)

			Conservative range		Wide range	
Obs	Adjustable parameters	Initial value	Lower bound	Upper bound	Lower bound	Upper bound
Q	Random roughness (rr, cm)	1.0	0.48	1.24	0.23	1.53
Q	Leaf area index (LAI, m^2/m^2)	1.0			0.65	1.50
Q & Qs	Manning's n of slope (n, -)	1.0	0.60	1.51	0.50	1.85
Q & Qs	Manning's n of Channel (chn, -)	1.0	0.60	1.51	0.50	1.85

Note: values were taken from literature (Cronshey, 1986; António José Dinis Ferreira, 1996; Nunes et al., 2017; Nunes et al., 2016; João Pedro Nunes et al., 2018; Nunes et al., 2009; Nunes et al., 2008; Serpa et al., 2015; Valente et al., 1997)

As for adjustable parameters related to soil types, two sets of parameter bounds were used: one represents all soil families in this catchment which were used in the sensitivity analysis of the model, and the other one represents the prominent soil families only which were used in the automatic calibration since Haplic Luvisols (LVh) and Chromic Luvisols (LVx) cover about 90% of the catchment.

Table S.3 Adjustable parameters related to soil types and parameter bounds (multiplication factor over the original parameter)

			All soil families				Major soil families			
			Conservative range		Wide range		Conservative range		Wide range	
Obs	Adjustable parameters	Initial value	Lower bound	Upper bound	Lower bound	Upper bound	Lower bound	Upper bound	Lower bound	Upper bound
Q	Saturated hydraulic conductivity (*K*sat, mm/h)	1.0	0.30	21.93	0.23	37.43	0.92	18.47	0.84	27.42
Q	Initial moisture content (thetai, -)	0.55 * θ_s			0.40 * θ_s	0.98 * θ_s			TWI	TWI
Q	Wetting front suction (psi, cm)	1.0	0.37	2.34	0.32	10.98	0.47	1.64	0.45	2.21
Qs	Grain size (d50, mu)	1.0	0.21	6.14	0.08	29.69	0.45	5.64	0.24	8.43
Qs	Cohesion (coh, kPa)	1.0	0.51	1.46	0.16	1.86	0.51	1.05	0.41	1.10
Qs	Cohesion of channel (chc, kPa)	1.0	0.51	1.46	0.16	1.86	0.51	1.05	0.41	1.10
Qs	Aggregate stability (ags, -)	1.0	0.07	1.77	0.06	2.26	0.34	1.06	0.23	1.12

Note: values were derived from literature (de Carvalho Cardoso, 1965; Nunes et al., 2008).

Table S.4 LISEM performance of each storm after event-based ensemble LISEM calibration for before and after the fire

		S1	S2	S3	S4	S5	S6	S8	S9	S10	S11	S12
Q	r^2	0.55	0.94	0.74	0.87	0.93	0.98	0.93	0.31	0.86	0.83	0.77
	NSE	0.53	0.83	-0.05	0.87	0.89	-0.27	0.85	-21.46	0.86	0.23	0.12
	PBIAS	-25.70	-34.40	-79.10	-12.60	29.80	93.80	31.90	151.80	-6.60	-82.30	16.40
Qs	r^2	0.61	0.28	0.87	0.53	0.95	0.93	0.97	0.37	0.55	0.55	0.62
	NSE	0.50	0.17	-34.64	0.37	0.91	-2.55	0.97	-32.07	0.33	0.03	0.04
	PBIAS	9.60	30.30	294.20	36.00	17.00	168.10	-0.90	338.10	-52.90	-80.10	13.00

Table S.5 LISEM performance of each storm for jack-knife cross-validation

		S1	S2	S3	S4	S5	S6	S8	S9	S10	S11	S12
Q	r^2	0.66	0.94	0.72	0.84	0.84	0.95	0.83	0.30	0.85	0.80	0.76
	NSE	0.59	0.82	-0.12	0.83	0.69	-0.14	0.53	-21.46	0.83	0.18	0.10
	PBIAS	-30.90	-36.20	-81.40	-11.90	39.00	89.80	51.90	150.60	-10.70	-84.30	16.90
Qs	r^2	0.73	0.21	0.86	0.47	0.90	0.89	0.96	0.42	0.58	0.60	0.64
	NSE	0.69	-0.14	-36.51	0.30	0.63	-3.41	0.89	-19.68	0.14	0.05	0.41
	PBIAS	-1.90	52.20	305.40	40.10	43.00	190.60	16.90	287.90	-65.90	-79.80	1.90

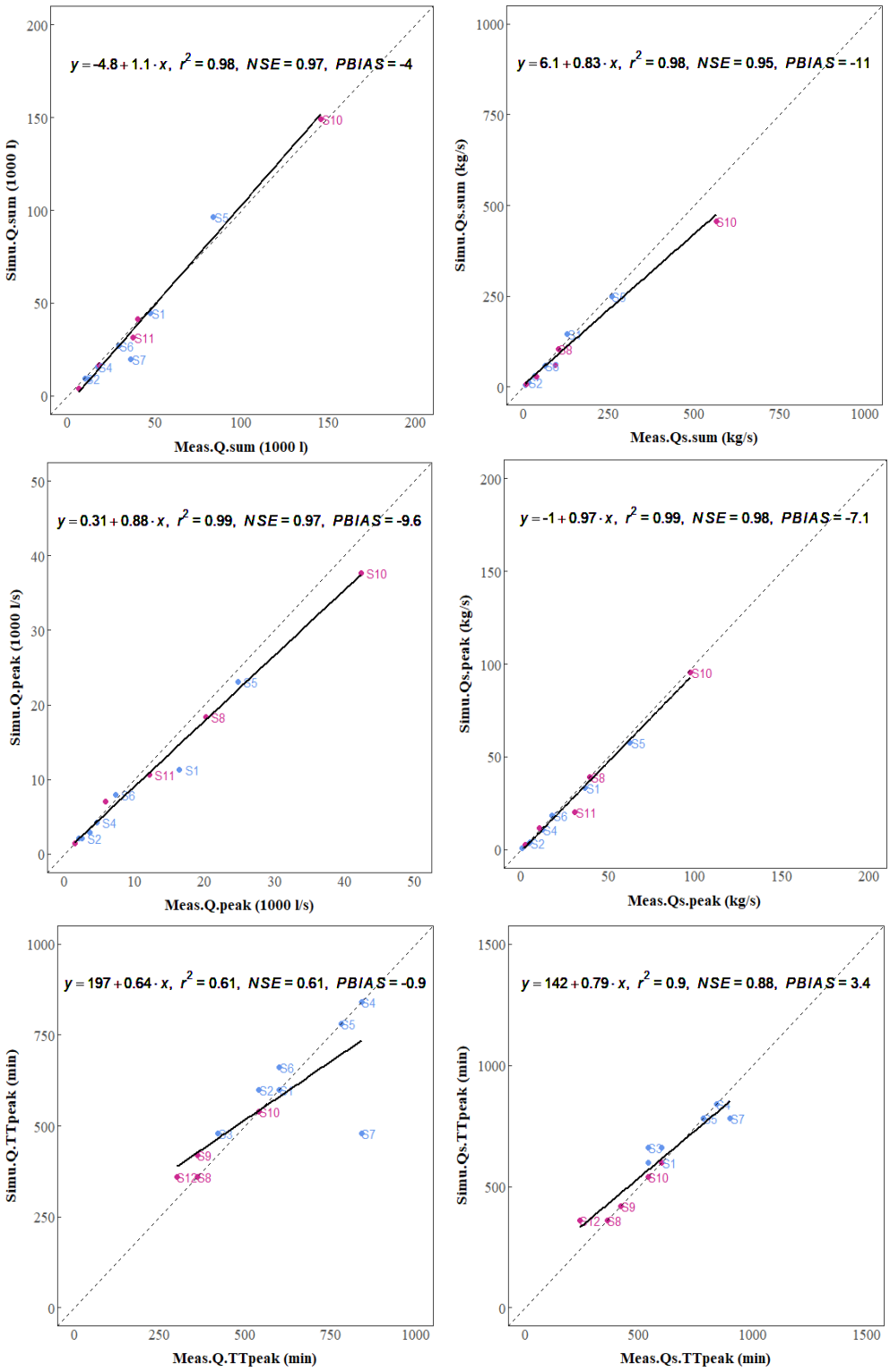

Figure S.1 Measured versus simulated results of all events after automated calibration at the catchment scale

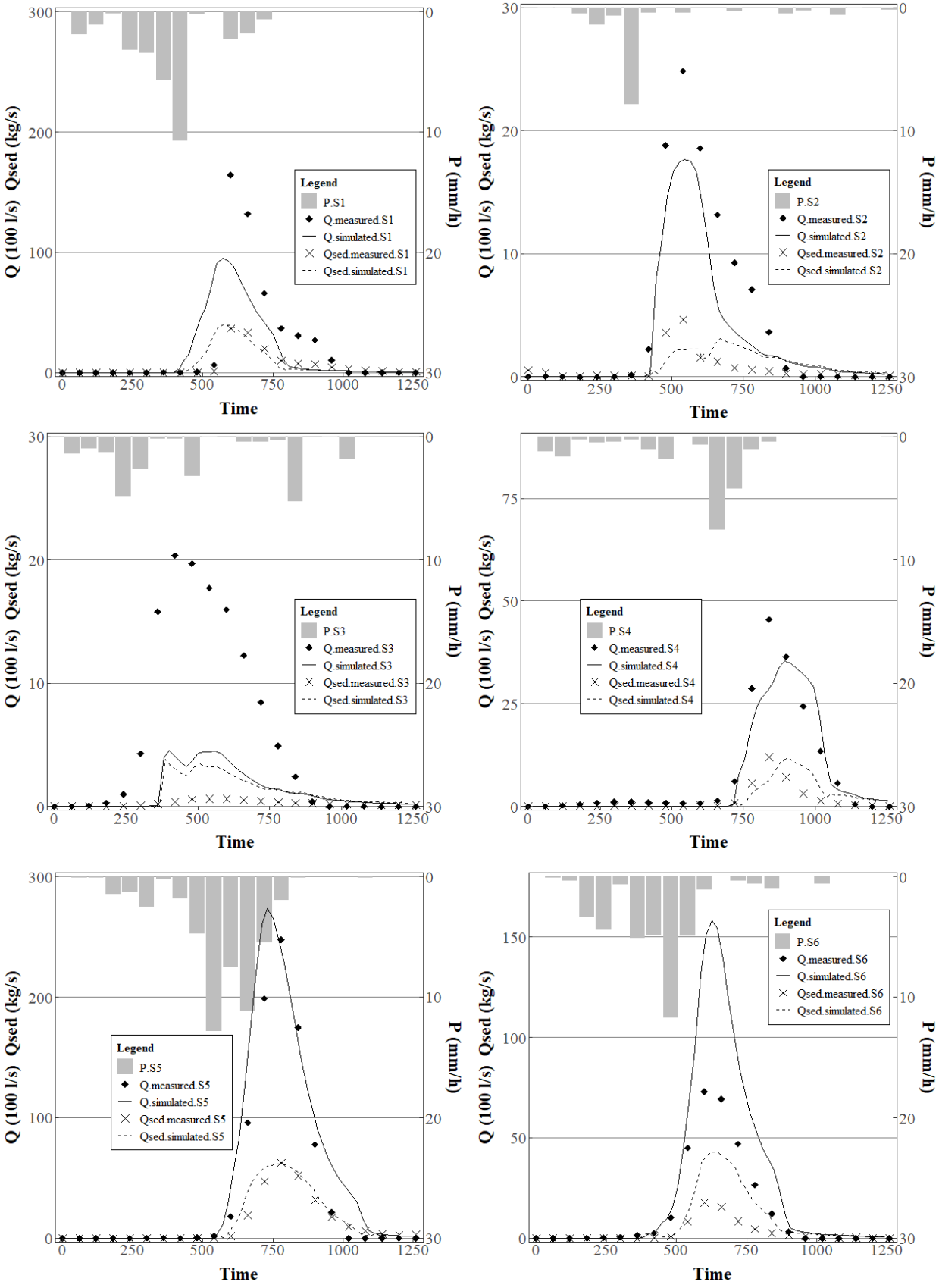
Q (100 l/s) Qsed (kg/s)
P (mm/h)
Time
Legend
P.S1
Q.measured.S1
Q.simulated.S1
Qsed.measured.S1
Qsed.simulated.S1
Legend
P.S2
Q.measured.S2
Q.simulated.S2
Qsed.measured.S2
Qsed.simulated.S2
Legend
P.S3
Q.measured.S3
Q.simulated.S3
Qsed.measured.S3
Qsed.simulated.S3
Legend
P.S4
Q.measured.S4
Q.simulated.S4
Qsed.measured.S4
Qsed.simulated.S4
Legend
P.S5
Q.measured.S5
Q.simulated.S5
Qsed.measured.S5
Qsed.simulated.S5
Legend
P.S6
Q.measured.S6
Q.simulated.S6
Qsed.measured.S6
Qsed.simulated.S6

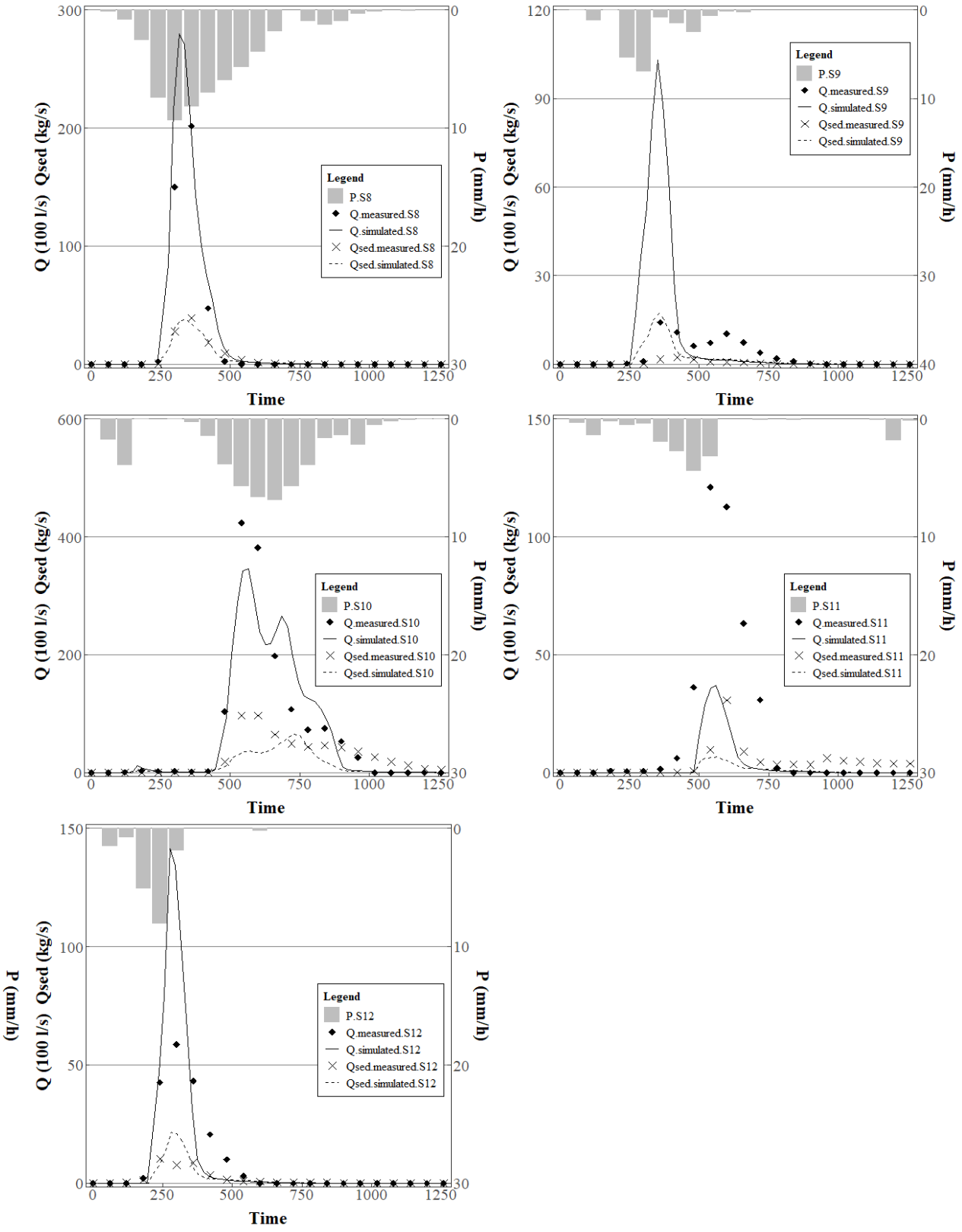

Figure S.2 Rainfall (P, right axis), discharge (Q, left axis) and sediment flow (Qs, left axis) at the Prado outlet for four events

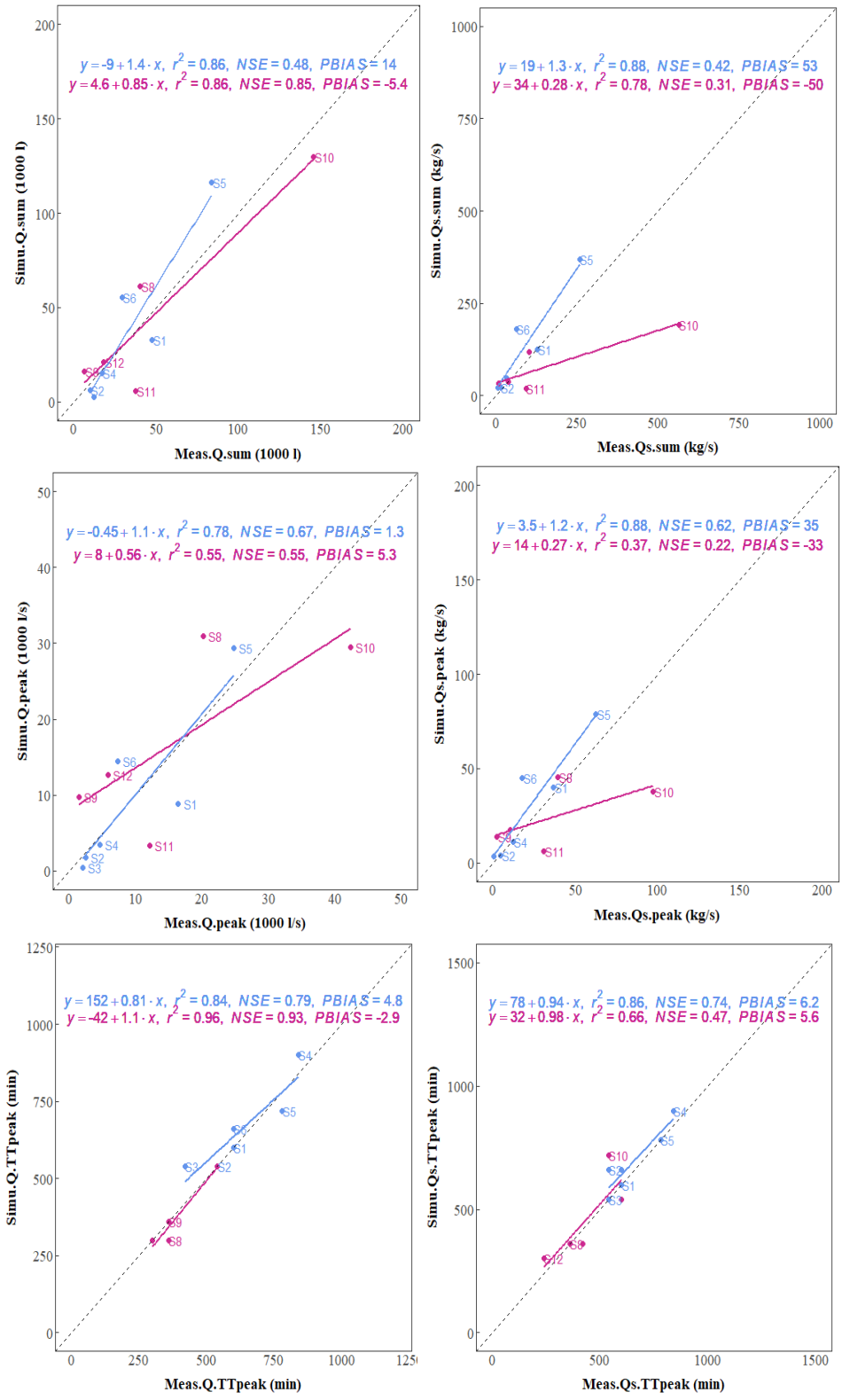

Figure S.3 Model performance in catchment hydro-sedimentary response simulations for jack-knife cross-validation (blue = Pre-wildfire; purple = Post-wildfire).

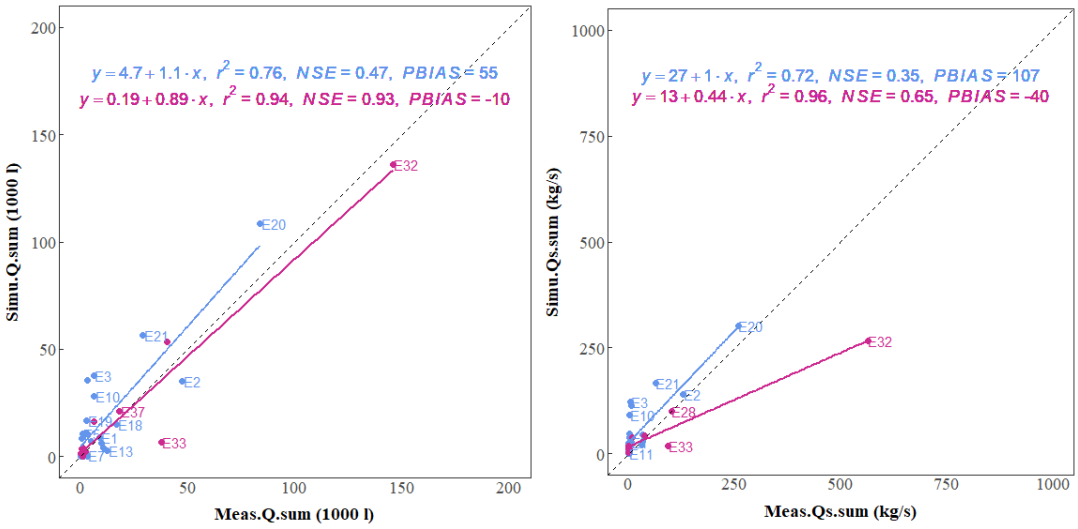

Figure S.4 Model performance in terms of predicting total discharge and erosion for all events during the study period (blue = Pre-wildfire; purple = Post-wildfire).

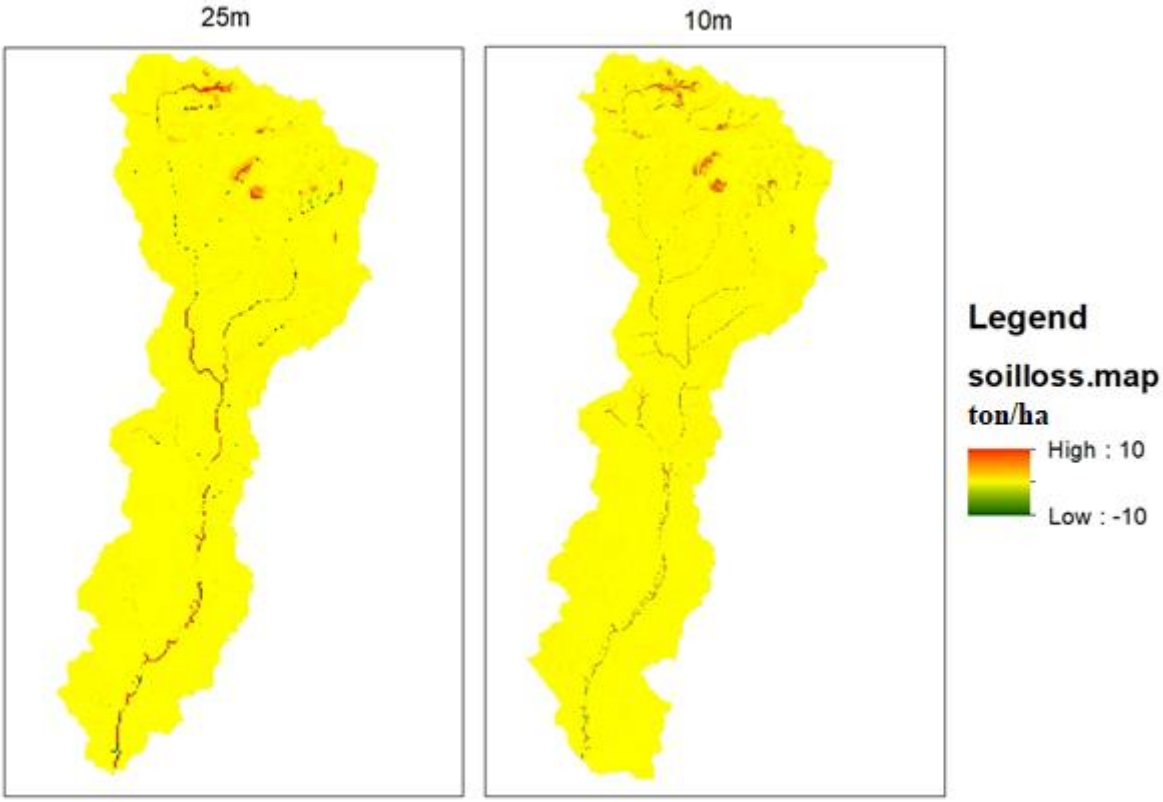

Figure S.5 Soil loss map of 25m vs 10m resolution